DEVELOPMENT OF AN AUTONOMOUS PROPULSION SYSTEM FOR SURFACE VESSELS

1 author:

Emerson Andrade
Federal University of Rio de Janeiro
5 PUBLICATIONS **1** CITATION

SEE PROFILE

UNIVERSIDADE FEDERAL DO RIO DE JANEIRO

ESCOLA POLITÉCNICA

CURSO DE ENGENHARIA NAVAL E OCEÂNICA

EMERSON MARTINS DE ANDRADE

DEVELOPMENT OF AN AUTONOMOUS PROPULSION SYSTEM FOR SURFACE
VESSELS

RIO DE JANEIRO

2020

EMERSON MARTINS DE ANDRADE

DEVELOPMENT OF AN AUTONOMOUS PROPULSION SYSTEM FOR SURFACE VESSELS

Projeto de Graduação apresentado ao Curso de Engenharia Naval e Oceânica da Escola Politécnica, Universidade Federal do Rio de Janeiro, como parte dos requisitos necessários à obtenção do título de Engenheiro.

Orientador: Prof. Joel Sena Sales Junior

Coorientador: Prof. Antonio Carlos Fernandes

RIO DE JANEIRO

2020

DEVELOPMENT OF AN AUTONOMOUS PROPULSION SYSTEM FOR SURFACE VESSELS

Emerson Martins de Andrade

PROJETO DE GRADUAÇÃO SUBMETIDA AO CORPO DOCENTE DO CURSO DE ENGENHARIA NAVAL E OCEÂNICA DA ESCOLA POLITÉCNICA DA UNIVERSIDADE FEDERAL DO RIO DE JANEIRO COMO PARTE DOS REQUISITOS NECESSÁRIOS PARA A OBTENÇÃO DO GRAU DE ENGENHEIRO.

Examinada por:

_____
Joel Sena Sales Junior, D.Sc. (COPPE/UFRJ)

_____
Antonio Carlos Fernandes, Ph.D. (COPPE/UFRJ)

_____
Carl Horst Albrecht, D.Sc. (COPPE/UFRJ)

_____
Dick K. P. Yue, Sc.D. (MIT)

RIO DE JANEIRO, RJ – BRASIL

OUTUBRO de 2020

Dedico este trabalho àqueles que de alguma forma cruzaram meu caminho e aos meus familiares que me incentivaram e estiveram sempre ao meu lado. Elaine, Mauricio, Mirelly e Gislainy: Amo vocês.

AGRADECIMENTOS

Agradeço aos meus pais que viabilizaram a minha estadia na cidade do Rio de Janeiro. Elaine e Mauricio, muito obrigado por acreditarem tanto em seu filho e pelo carinho que sempre me foi dado.

Agradeço à minha família, sem os quais a vida não teria sentido e que sempre me receberam com devida alegria e amor. Um forte abraço para vocês.

Agradeço a todos os amigos que fiz durante essa longa jornada, em especial, aos meus numerosos irmãos e irmãs de Moradias, de Curso, da Equipe Minerva Aerodesign, Equipe Solar Brasil, Pólo Náutico e do Laboratório de Ondas e Correntes, obrigado pela amizade e que os momentos que vivemos juntos nunca saiam das nossas lembranças.

Finalmente, agradeço ao povo brasileiro que me proporcionou uma formação gratuita e de qualidade, das maiores que já pude presenciar.

Simplicity is the ultimate sophistication.

Leonardo da Vinci

RESUMO

O presente trabalho teve por objetivo realizar o desenvolvimento de um sistema de propulsão autônomo que seja intercambiável entre embarcações de superfície de pequeno porte.

A metodologia de trabalho envolveu a revisão da literatura sobre sistemas autônomos, a fim de se obter um panorama geral da evolução das soluções para pequenas embarcações. O trabalho foi desenvolvido tendo como referência o perfil operacional da embarcação e recursos tecnológicos que podem ser adquiridos no Brasil. Além disso, o trabalho envolveu a seleção de propulsores, periféricos eletrônicos, programas e controle de sistemas.

O objetivo foi o desenvolvimento, verificação e validação de uma solução de sistema de propulsão autônoma para embarcações de superfície de pequeno porte.

Por fim, foi obtido um sistema com excelente comportamento em águas calmas e razoável em alguns casos com ondas e ventos. As simulações foram capazes de gerar ótimos resultados que nos permitiram avaliar o desempenho da plataforma autônoma em várias circunstâncias.

Palavras-chave: Propulsão, Embarcações Autônomas, ROS, Robótica.

Abstract of the Course Conclusion Project presented to the Department of Naval and Ocean Engineering of the Polytechnic School as a partial fulfillment of the requirements for the degree of Bachelor in Naval and Ocean Engineering (B.Sc.)

Development of an Autonomous Propulsion System for Surface Vessels

Emerson Martins de Andrade

Advisor: Joel Sena Sales Junior, D.Sc.
Course: Naval and Ocean Engineering

Abstract
The present work aimed to develop an autonomous propulsion system that is interchangeable between small surface vessels.
The work methodology involved the literature review of autonomous systems, in order to obtain an overview of the evolution of solutions for small boats. The work was developed with reference to the vessel's operational profile and technologies that can be procured in Brazil. In addition, the work involved the selection of engines and propellers, as well as the selection of electronic peripherals, software and systems control.
The objective was the development, verification and validation of an autonomous propulsion system solution for small surface vessels.
Finally, a system with excellent behavior in calm water and reasonable behavior in some cases with waves and winds was obtained. The simulations were capable to generate great results that allowed us to evaluate the performance of the autonomous platform against various circumstances.

Keywords: Propulsion, Autonomous Vessel, ROS, Robotics.

List of figures

List of tables

TABLE OF CONTENTS

1 INTRODUCTION

1.1 Context of study

Nowadays, the use of autonomous systems is rapidly increasing, and the modularity approach and the use of simulations are more and more appreciated. In contrast, non-flexible systems and experimental tests are very expensive and need careful management. Numerical solutions, in this case, are more adequate due to the fact of the speed of implementation, the costs involved and the ease to change and test. Therefore, the application of Naval Architecture and Ocean Engineering concepts mixed with Robotics tools can generate magnificent solutions and reduce the risk of failure of the real application.

1.2 Purpose of study

Check a ship's loaded draft requires visual access to all draft marks. However, such access is not always easy to perform, and in addition, the presence of waves and other vessels can make human perception of the correct draft mark difficult, since the oscillation of the free surface makes it difficult to identify its average position next to the draft mark. Similar difficulties occur with the case of verifying the integrity of the anchoring lines and in this case, for instance, the use of an autonomous vessel together with an ROV would make easier the tasks of visualization and inspection.

Finally, this kind of solution is justified by the growing demand for safety, reliability and improve offshore processes. The tests will be carried out using computer resources for numerical simulation. This study focused on the autonomous propulsion solution, and the verification of draft and line integrity cases will be simulated and analyzed in order to verify the correct representation and performance of the applied method.

1.3 Organization

In order to give an overview of how the project was organized and executed, this section provides the steps in which this work followed, each one with a brief explanation.

- **Section 2** starts with a brief literature review about autonomous systems and also discusses the main idea of design methodology;

- **Section 3** describes the design framework used and its considerations about the expectations of this autonomous system. The operational profile of the system is also defined here, where we show the idea of tasks that can be performed;

- **Section 4** has all the development of the system, showing the selected items, physical properties of the system, software, and control system;

- **Section 5** describes with detail the simulations carried out based on the operational profile of the vessel and its properties developed in Section 4;

- **Section 6** shows and discusses all the results of the tasks and station-keeping simulations;

- **Section 7** has a conclusion about all the results of this project.

2 REVIEW

First of all, it is important to give a definition of the term "autonomous vehicle" to avoid any kind of mistakes and discussion about how much "intelligence" is needed to be considered autonomous. Based on [1], the definition as follows:

> "*...all relevant vehicles that do not have a human on board. Moreover, an autonomous vehicle is an unmanned vehicle with some level of autonomy built in — from teleoperations to fully intelligent systems.*"

With this definition on the mind, it is time to know more about this technology and its evolution through time.

2.1 Literature Review

In this section, we highlight the main events that occurred in the autonomous vehicles field (which includes the autonomous vessels) since ancient times.
There is no exact date or inventor responsible for the first form of automated steering, the auto-tiller. What is known is that this device equipped sailboats since a long time ago, using ropes to connect something like a weathervane to the boat's tiller, so that the craft stays on course even with shifting winds [2]. After this, a lot of advances were made and the main ones are described below:

1478 - Sketch of a pre-programmed clockwork cart by Leonardo Da Vinci. The clever control mechanism could have taken the vehicle through a predetermined course [3];

1788 - James Watt designs the first governor, or speed limiter - a feedback-control system - for steam engines [4];

The 1860s - Robert Whitehead invented the self-propelled torpedoes that initially had only simple guidance systems for keeping a constant course and depth [5];
The 1930s - "Mechanical Mike" Autopilot, Wiley Post became the first person to fly solo around the world [6];

The 1940s - US Navy used a USV to radioactive measurement at the South Pacific islands [1];

The 1960s - Experimental robots were navigating through novel environments at SRI and Stanford (Stanford Artificial Intelligence Laboratory Cart), testing out still-new AI techniques [7];

The 1980s - German pioneer Ernst Dickmanns got a Mercedes van to drive hundreds of highway miles autonomously [8];

The 1990s - US Navy developed and tested more sophisticated USV mine sweeping systems [9];

The 2000s - Some companies were founded and the US Navy started several new USV programs. The Office of Naval Research (ONR) provided funding to the US Naval Facilities Engineering Support Center (NFESC) to develop a small USV sea target called Sea Fox [10].

2.2 Design Methodology

This description of the method outlines the bases studied in Introduction to Design Theory and to concentrate more on the practices, decisions and experiences lived during the development of this project.

In Naval Engineering, it is a common understanding that the preliminary design can be represented by the first loop in the design spiral (Figure 1) proposed by Evans [11]. The intention of this design process is not to fully assume Evans's proposal and design method philosophy, which is open to criticism. However, the purpose of referencing the author is to endorse that, as can be seen in the outermost spiral - the first lap - it is not necessary to carry out all syntheses (or analyzes, as in some cases), but those that contribute to the understanding of the preliminary project are carried out.
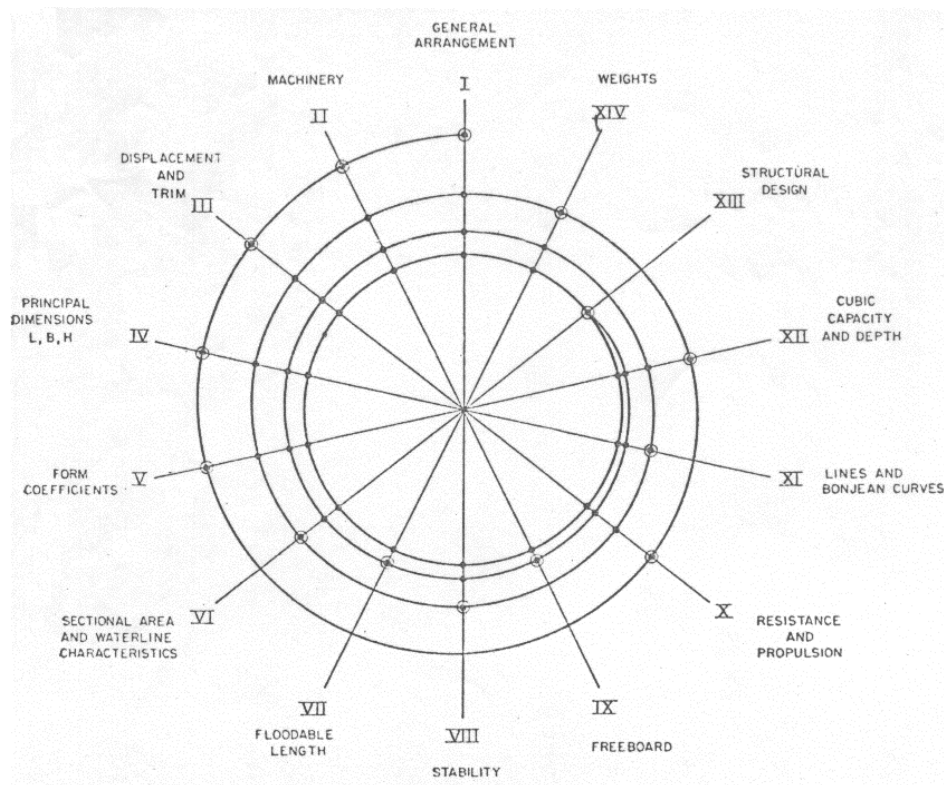
Figure 1 - Project spiral proposed by Evans [11].

3 METHODOLOGY

3.1 Design Framework

The Design Framework is a strategy for streamlining the process and reflective action on the factors that influence the object. The framing action must recognize these factors and understand how they interact to produce the desired object. These factors are the expectations that the object must attend.

The Global Expectations are characteristics underlying the project that must be considered and met, through criteria, by the object. Global Expectations have an order of precedence and relevance among them. Design choices that spell out trade-offs must first meet the most important expectations. For the project in question, three Global Expectations were chosen:

1. Adaptability
2. Good operability
3. Safety

The Synthesis Elements chosen were:
1. General arrangement: the arrangement of the system's equipment, compartments and installations;
2. Control System: equipment responsible for sensing, processing and control the system;
3. Communication system: equipment responsible for transmission and reception of information;
4. Electrical system: equipment responsible for the storage, transmission and management of energy;
5. Propulsion system: equipment that operates to propel the vessel (thrusters, engine, tail);
6. Structure: reinforcement arrangement and dimensioning that assist in maintaining the physical-structural integrity of the system.

The relationships between the Synthesis Elements and the Global Expectations were defined so that it is possible to identify the influence of each element on what is desired from the project. Then, for each element present in each Global Expectation, a Specific Expectation was defined that represented the influence of the element for that Global Expectation. Figure 2 shows the Synthesis Elements and the relationships between the elements and the expectations.
Table 1 shows the complete framework.
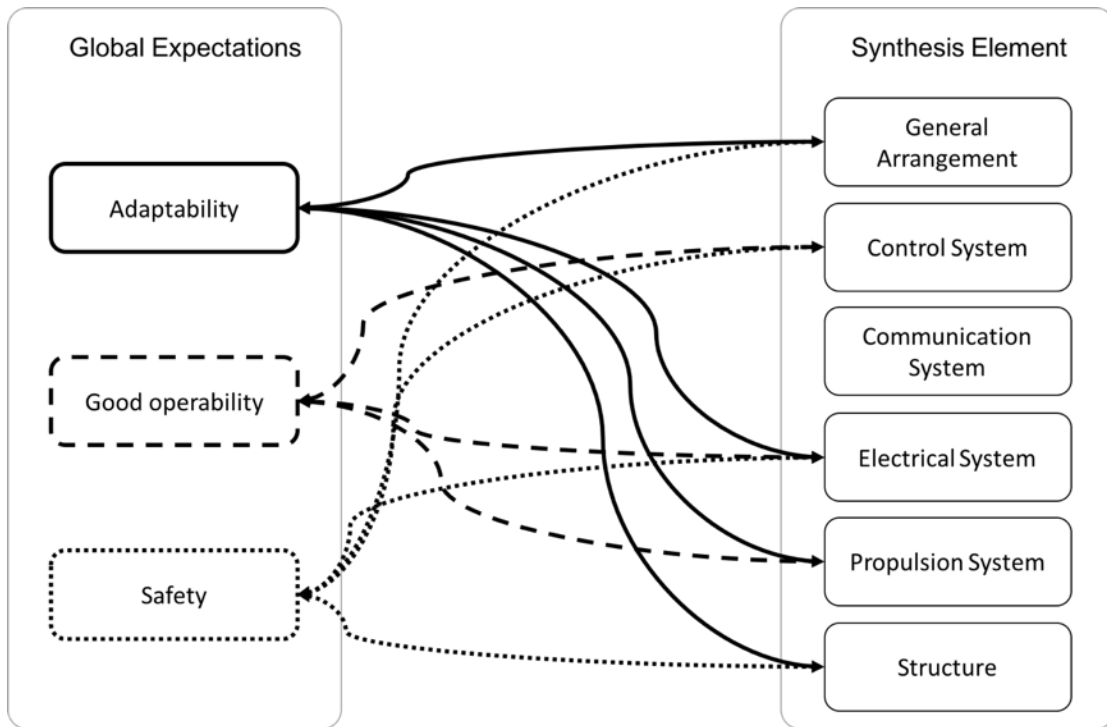
Figure 2 – Relationship between Global Expectation and Synthesis Elements.

Table 1 – Complete Design Framework

Global Expectations		Synthesis Elements	Specific Expectations
Adaptability	Hull	General Arrangement	*Be easy to install on any type of hull*
		Electrical System	*Have an easy physical expansion system*
		Structure	*Be physically expandable*
	Equipments	General Arrangement	*Have spaces for installing external equipment*
		Electrical System	*Have an expandable and modular plug and play (PnP) system*
	Enviroments	Control System	*Being able to deal with various environmental conditions*
		Communication System	*Have good communication in different environments*
		Propulsion System	*Ensure a good response/thrust in different environments*
Good operability	Navigation	Control System	*Ensure a response similar to the desired*
		Propulsion System	*Ensure good maneuverability*
	Energetic Autonomy	Electrical System	*Ensure good management of available energy*
		Propulsion System	*Reduce consumption whenever possible*
Safety	Structural	Structure	*Ensure that the structure supports system loads*
	Electrical	Electrical System	*Ensure the correct dimensioning of the electrical system*

Stability	General Arrangement	*Ensure the required stability as a rule*
Navigation	Control System	*Ensure the correct dimensioning of the control system*

3.2 Operational Profile of the Vessel

In this section, we are interested in define some characteristics of the vessel based on tasks that it will have to perform. In a few words, the vessel must be launched close to a target vessel (e.g., an FPSO - Floating Production Storage and Offloading) and execute the desired task, in the present case checking draft marks (Figure 4) or verifying the integrity of anchoring lines (Figure 3). Similarly to Zoss [12], it is clear that for these tasks maneuvering capabilities will be more important than speed, so, the maximum speed during the tasks will be limited to 3 knots (approximately 1.5 m/s) and the endurance will be assumed 6 hours in this speed.
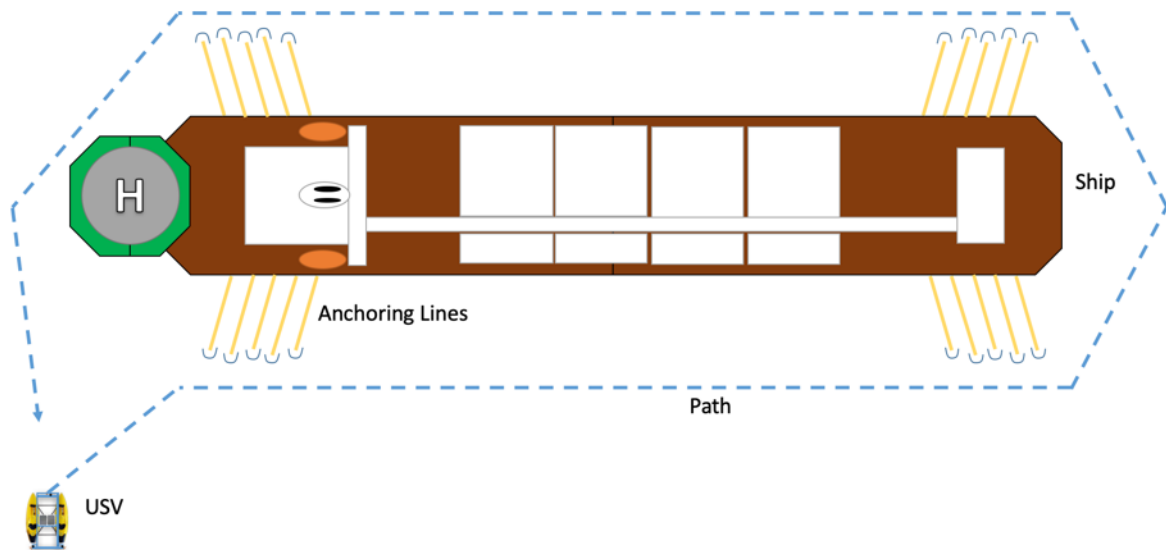
Figure 3 – The idea to verify the integrity of anchoring lines. The blue dashed line represents the path to be followed by the system.
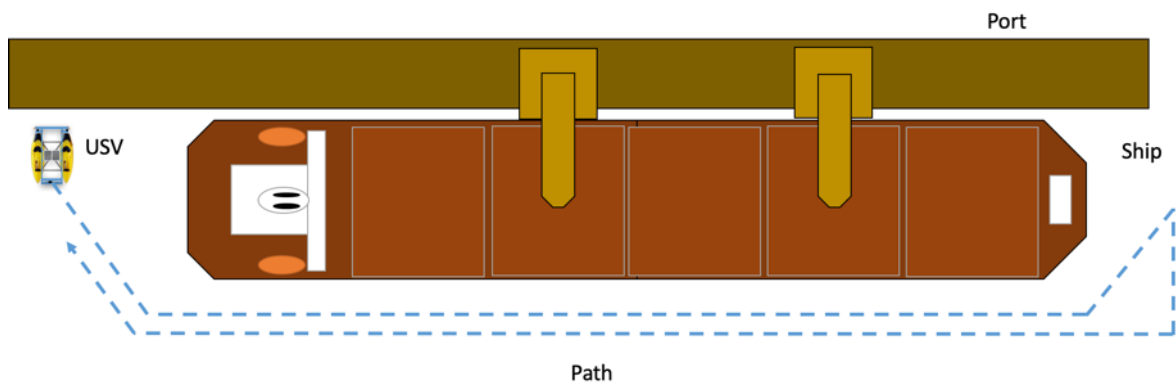
Figure 4 - Idea to check draft marks during the loading in the port. The blue dashed line represents the path to be followed by the system.

4 SYSTEM DESIGN

4.1 Development

4.1.1 Hull

In order to choose a specific configuration of hulls to be used as a platform to the propulsion system, some research was done and as discussed in Murdijanto [13] and Luhulima [14], the multihull configurations show almost similar motion characteristics as compared to the monohull up to sea state 3 (wave height from 0.5 to 1.25 meters), but the multihull has some advantages compared to monohull type, having wider deck area, better transverse stability and in a certain case, it could reduce total resistance. Based on this, the multihull configuration was chosen, more specifically, a catamaran one.

The idea is choosing existing components, avoiding to be only a theoretically project. After some searching here in Brazil, the "Kayak Wave" (Figure 5) was selected to be used as a catamaran hull. Unfortunately, there are few suitable options and this one is exactly on the ranges of length defined previously. The main characteristics of this hull are presented in Table 2.

Table 2 - Kayak Wave main properties

L (m)	2.45
B (m)	0.60
H (m)	0.30
Weight (kg)	14.00
Capacity (kg)	85.00

Figure 5 - Kayak Wave. Source: https://www.caiaker.com

Although a complete catamaran solution was not found with some adaptations is possible to transform two Kayak hulls in a multihull configuration. The space between the hulls will be considered the same of hull beam and the final characteristics of the catamaran configuration is showed in Table 4 and Figure 6.

Table 3 - Light weight items.

Item	Qty	Mass/each (kg)	Total Mass (kg)
Hull	2	14.0	28.0
Aluminium Beams	1	4.0	4.0
Electronics	1	2.0	2.0
Motors	3	12.0	36.0
Battery	1	27.5	27.5
		TOTAL (kg)	97.5

Into the light weight was considered an additional 2 kg to the Electronics and 4.0 kg due to reinforcements and bars that joined the hulls and will serve as the base to electronic components box (Figure 6 and Table 3).

Table 4 - Catamaran main characteristics

L (m)	2.45
B (m)	1.80
H (m)	0.30
Capacity (kg)	168.00
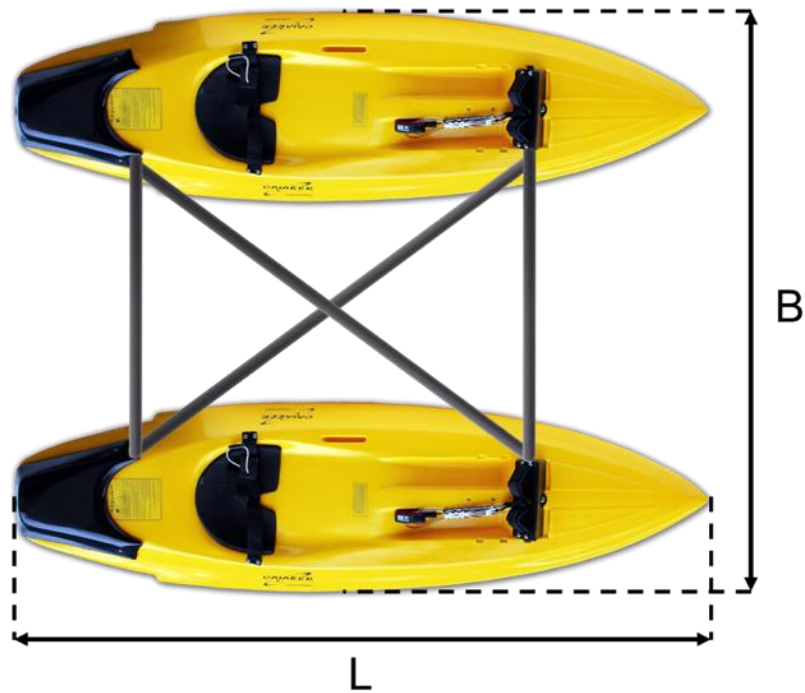
Figure 6 - Kayak Wave.

4.1.2 Propulsion Frame

This part is the main objective of this project and is composed of some structural aluminum beams (Figure 7), three electric outboard motors (Figure 9) and a box (Figure 10) with the electronics components (discussed with details in section 4.2 Hardware and Electronics).

Figure 7 - Structural aluminium beams. Source: https://www.flexlink.com

The thruster force characteristics were found in Magalhães [15] and are present in Table 5. A polynomial adjustment to the thuster's static test points was done and is shown in Figure 8.

Table 5 - Thruster's static test results. Source: Magalhães [15]

Cell Voltage (V)	Armature Voltage (V)	Cell Force (kgf)	Current (A)	Power (W)
1.40	-0.12	-0.15	-0.88	0.11
1.45	-1.00	0.09	-2.42	2.42
1.40	-1.49	-0.15	-2.73	4.06
1.38	-2.00	-0.25	-3.33	6.67
1.32	-2.50	-0.55	-3.94	9.85
1.27	-3.00	-0.80	-4.67	14.00
1.23	-3.50	-1.00	-5.45	19.09
1.26	-4.00	-0.85	-6.42	25.70
1.18	-4.50	-1.25	-7.55	33.95
1.13	-5.00	-1.49	-8.76	43.79
1.11	-5.50	-1.59	-9.61	52.83
0.90	-6.00	-2.63	-10.67	64.00
0.82	-6.50	-3.03	-11.91	77.41
1.40	0.00	-0.15	0.06	0.00
1.41	0.50	-0.08	2.33	1.17
1.41	1.00	-0.12	2.07	2.07
1.43	1.50	0.01	2.54	3.81
1.42	2.00	-0.07	3.17	6.35
1.42	2.50	-0.05	3.70	9.26
1.42	3.00	-0.07	4.33	12.99
1.49	3.50	0.29	5.04	17.65
1.49	4.00	0.29	5.84	23.37
1.52	4.50	0.44	6.62	29.80
1.56	5.00	0.63	7.55	37.73
1.60	5.50	0.84	8.48	46.65
1.68	6.00	1.21	9.58	57.51
1.68	6.50	1.22	10.66	69.31
1.71	7.00	1.36	11.63	81.41
1.78	7.50	1.73	12.77	95.80
1.81	7.96	1.87	14.02	111.61
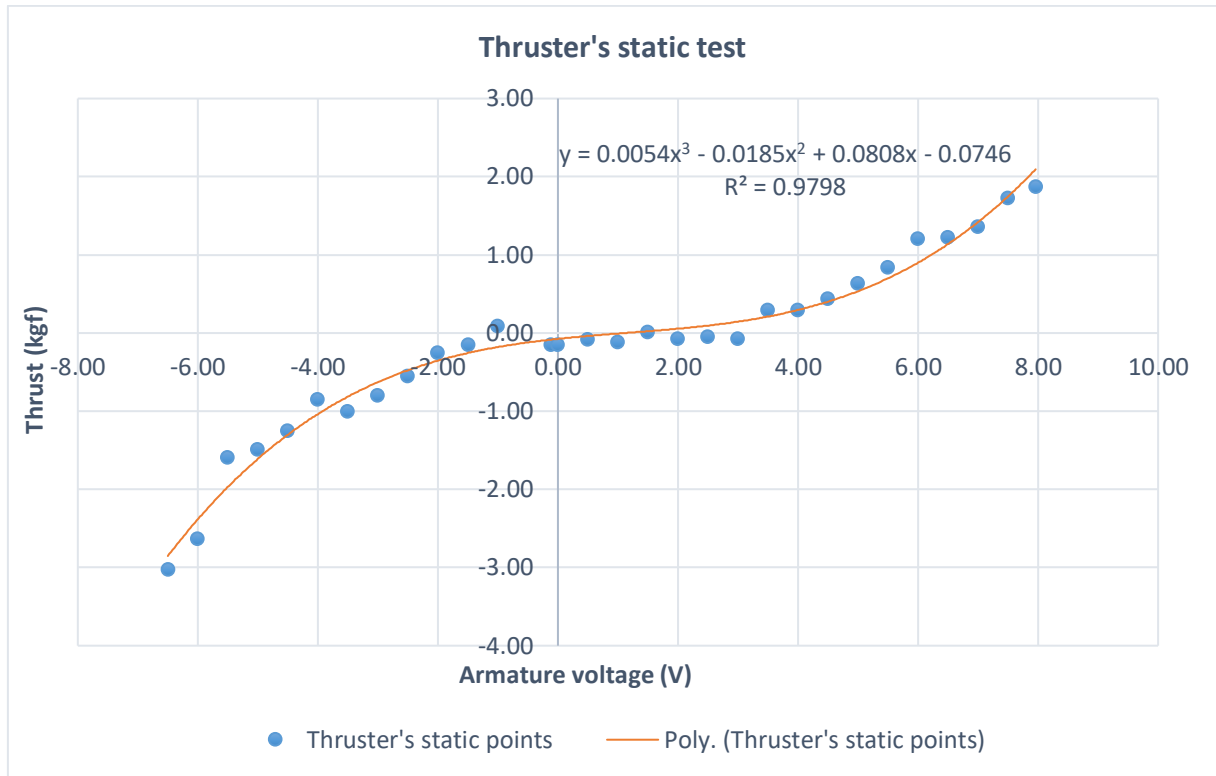
Figure 8 - Polynomial adjustment to the thuster's static test points. Source: Magalhães [15].

Figure 9 - Phantom electric outboard motor. Source: http://www.targetadventure.com.br

Figure 10 - Hermetic box. Source: https://produto.mercadolivre.com.br/MLB-1108142369-caixa-hermetica-

multiuso-master-grande-35x42x15-preta-chm014-_JM

The structural aluminum beam was chosen due to its high adaptability, meaning that if we need to assembly the same system to other kinds of hulls (bigger, small, monohull, etc.) it is possible. Three Phantoms model 34lbs marine motors were selected as thrusters due to the easy access in Brazilian stores, where there are not many options. In addition, its thruster capacities were studied by Magalhães [15]. A hermetic box was selected to stay above the aluminum frame to protect electronic devices from environmental hazards. All these components will be part of the autonomous propulsion system proposed in this work and the initial idea can be observed in Figure 11.
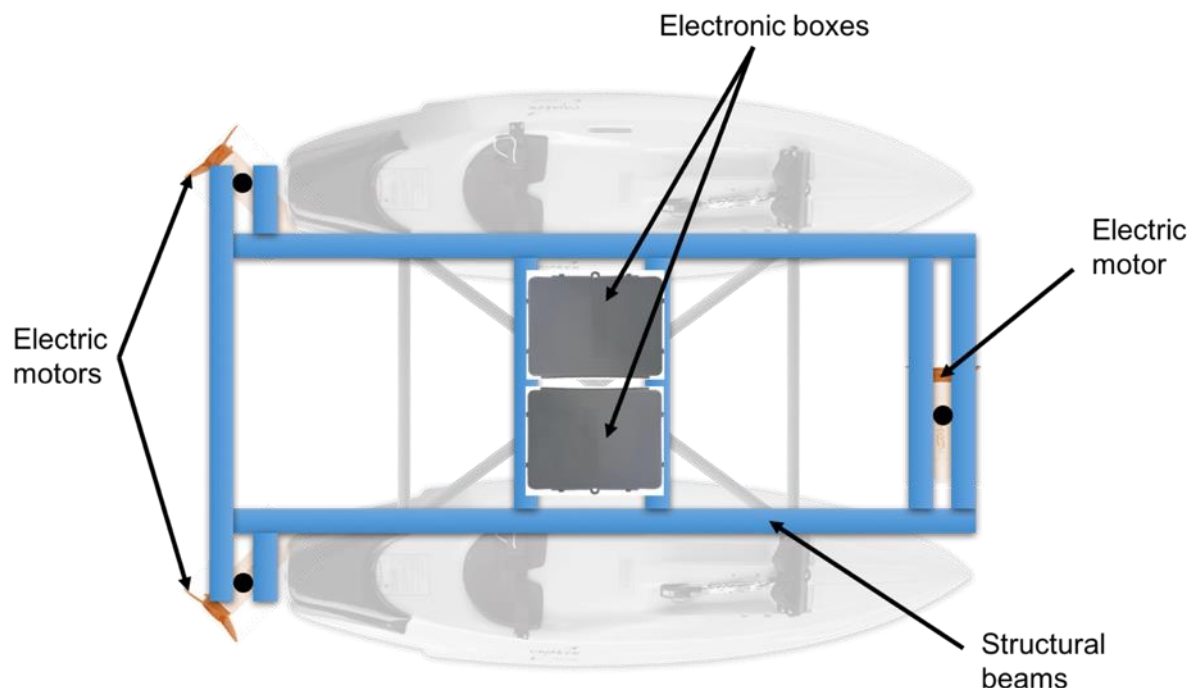
Figure 11 - Preliminary arrangement of the autonomous propulsion system.

4.1.3 Vectored Propulsion

The propulsion arrangement proposed set stern motors with 45 degrees from the centerline and the bow thruster with 90 degrees (Figure 12).
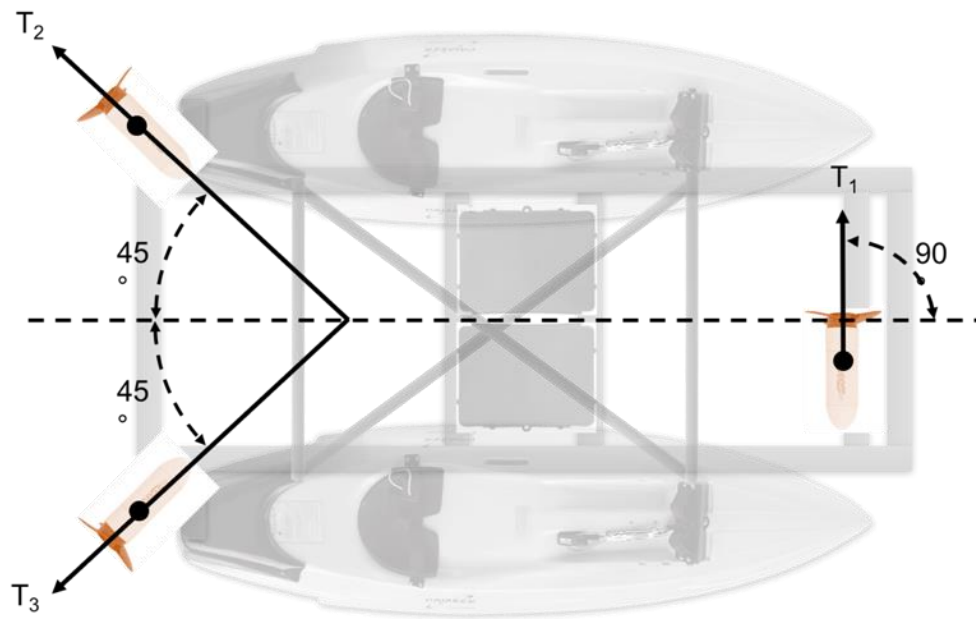
Figure 12 - Thuster's configuration.

With this configuration the system is able to perform maneuvers and station keeping without the need of such a mechanism to rotate the motors (e.g. azimuth thruster).
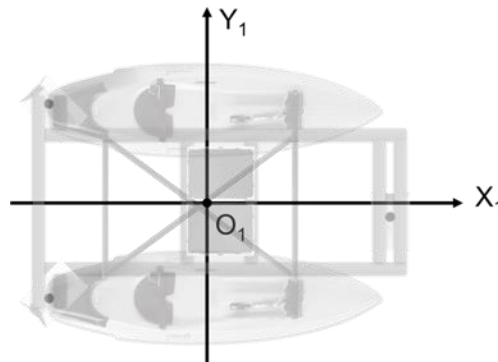
Figure 13 - Local coordinate system (O_1, X_1, Y_1).

To distribute the forces and moments required by the control system, a thrust-allocation algorithm proposed by Sørdalen [16] is used. This thrust-allocation scheme helps significantly to reduce the power consumption for the dynamic positioning of vessels when rotatable azimuth thrusters are used. In the present case, the thrusters have a fixed orientation and this simplifies the problem. However, some power will be lost due to this fact.

The local coordinate system (O_1, X_1, Y_1) adopted is presented in Figure 13, where X_1 is aligned with the longitudinal vessel direction, Y_1 with the transverse direction and O_1 is located at midship (Lwl/2).

Each thruster can be defined by:

- $x_{thruster}^i$ thruster coordinate on axis O_3X_3

- $y_{thruster}^i$ thruster coordinate on axis O_3Y_3

- $\alpha_{thruster}^i$ thruster angle

- T^i_{max} thruster maximum thrust
    - in the present work there are 3 thrusters, so, $i = 1, 2, 3$.

And the system used to solve this allocation is defined as follows:

$$A \cdot T = \tau \tag{1}$$

$$T = [T_1, T_2, T_3]^T \tag{2}$$

$$A = \begin{bmatrix} c_1 & & c_3 \\ s_1 & \dots & s_3 \\ -c_1 \cdot y^1_{thruster} + s_1 \cdot x^1_{thruster} & & -c_3 \cdot y^3_{thruster} + s_3 \cdot x^3_{thruster} \end{bmatrix} \tag{3}$$

Where $c_1 = \cos(\alpha^i_{thruster})$ and $s_1 = \sin(\alpha^i_{thruster})$.

$$\tau = [\tau_x, \tau_y, \tau_\psi]^T \text{ and } \tau_c = [\tau_{xc}, \tau_{yc}, \tau_{\psi c}]^T \tag{4}$$

$$\tau = \begin{bmatrix} \sum_1^3 T_i \cdot \cos(\alpha^i_{thruster}) \\ \sum_1^3 T_i \cdot \sin(\alpha^i_{thruster}) \\ \sum_1^3 -T_i \cdot \cos(\alpha^i_{thruster}) \cdot y^i_{thruster} + T_i \cdot \sin(\alpha^i_{thruster}) \cdot x^i_{thruster} \end{bmatrix} \tag{5}$$

Where A is a matrix that depends on the thruster locations and is a function of the azimuth angles α. The thrust from each thruster is represented by T and the forces of surge, sway and the moment in the yaw direction are denoted by τ. The commanded forces and moment from the controller are denoted by τ_c.

Finally, the optimal solution can be found using the pseudo-inverse method (least squares) and the performance factor Q. According to Tannuri [18], this factor helps to compare the performance of different configurations of DP systems and is defined as:

$$Q = \sum_1^3 T^{i^{3/2}} \tag{6}$$

The factor used in the optimization algorithm is proportional to the square, not to the 3/2 of power. With this, Q can be minimized using a quadratic optimization and satisfying the boundary conditions, where:

$$\min (Q(T)) \tag{7}$$

Subject to:

$$A(\alpha) \cdot T = \tau_c \tag{8}$$

$$T_i \leq T_{max}^i \qquad (9)$$

In our case, as we have three thrusters with no angles α varying, we don't need to use the last steps of the optimization algorithm.

4.1.4 Center of Gravity and Inertias

The position of each item was defined following Figure 14 reference. To calculate the inertias, all items were considered as a point mass.
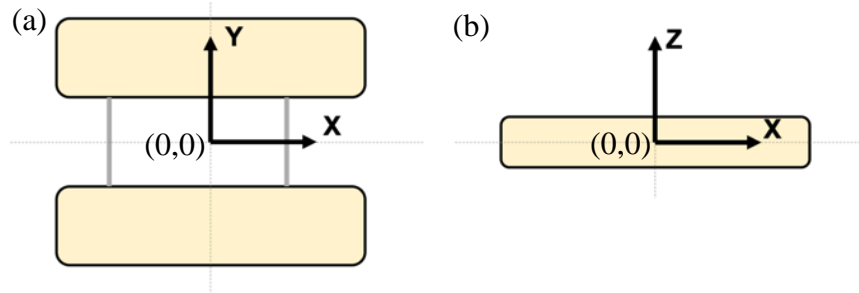
Figure 14 - Reference used to calculate de CoG. (a) Top view of the two hulls, plan XY. The initial point in X is at midship, and in Y is the plane of symmetry. (b) Side view of the hull, plan XZ. The initial point in Z is half of the hull height (0.5 * 0.30 = 0.15 m from hull bottom).

Table 6 - Position and mass of each component.

Item	Mass (kg)	X_{CG} (m)	Y_{CG} (m)	Z_{CG} (m)
Left Hull	14.00	0.00	0.60	0.00
Right Hull	14.00	0.00	-0.60	0.00
Electronic Box	2.00	0.00	0.00	0.20
Left Thruster	12.00	-1.25	0.60	-0.45
Right Thruster	12.00	-1.25	-0.60	-0.45
Center Thruster	12.00	1.25	0.00	-0.45
Battery	27.50	0.55	0.00	0.20

As can be observed in Table 7, the weights and positions from Table 6 were used to estimate the CoG (Center of Gravity) and the Inertias on each of the main axis.

Table 7 - Total mass, CoG and Inertia of the set.

Mass	97.50	**kg**
X_{CG}	0.00	**m**
Y_{CG}	0.00	**m**
Z_{CG}	-0.10	**m**

I_{XX}	26.31	**kg.m2**
I_{YY}	72.16	**kg.m2**
I_{ZZ}	83.29	**kg.m2**

4.2 Hardware and Electronics

This subsection aims to briefly describe the hardware components that compose the system. It also reports the connections between these devices and the type of communication used.

4.2.1 Single-Board Computer (SBC)

To give computer capacity to the system a Raspberry Pi 4 Model B (Figure 15) was chosen to integrate the hardware system. With this low-cost computer is ease communicate with peripherical sensors (e.g. GPS), do calculations and running the ROS middleware.
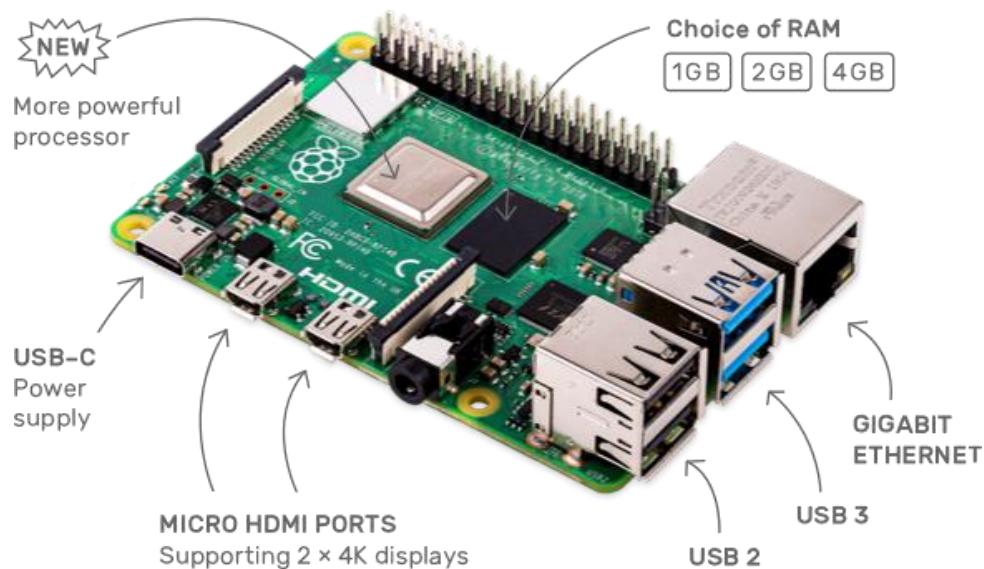
Figure 15 - Characteristics of Raspberry Pi 4 model B. Source: https://www.raspberrypi.org

In addition, it is also possible to integrate more sensors/systems as those described in this work, for instance, camera, water quality modules, bathymetry, accelerometer, temperature, etc.

4.2.2 Single-Board Microcontroller (SBM)

To give more flexibility an Arduino MEGA 2560 (Figure 16) was selected to serve as a microcontroller. In contrast with the SBC that is good at software applications, this board makes hardware projects simple.
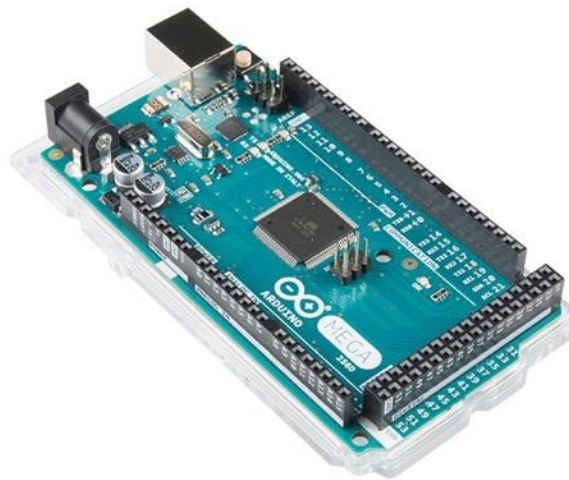
Figure 16 - Arduino MEGA 2560 board. Source: https://www.sparkfun.com

4.2.3 Positioning

To localize the system a GPS module is needed and to do this an Adafruit Ultimate GPS Breakout unit (Figure 17) was chosen. Its accuracy using the standard system is less than 3m for the position and 0.1m/s for velocity. These accuracies values can be better (centimeters of accuracy) using RTK (Real-Time Kinematic) technique or enabling the DGPS (Differential GPS) system.
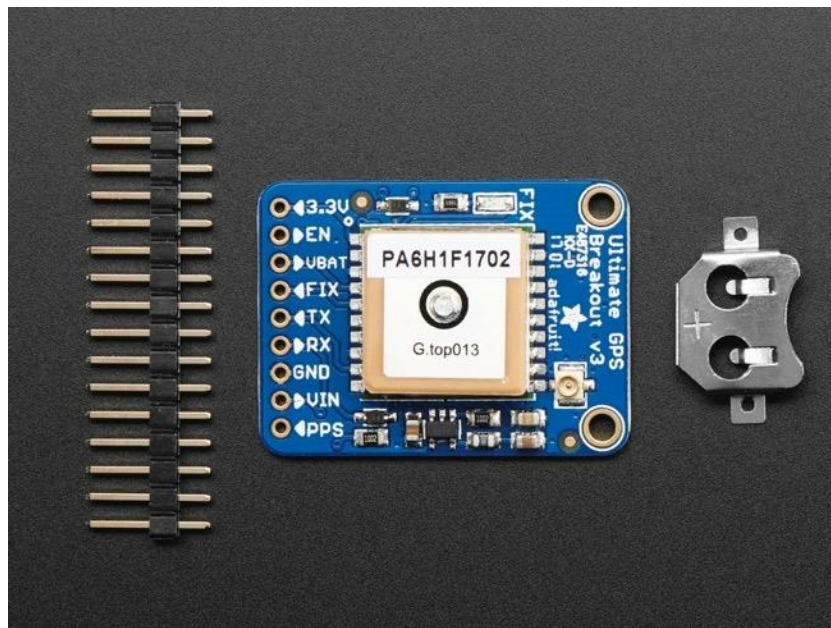
Figure 17 - Adafruit Ultimate GPS Breakout unit. Source: https://www.adafruit.com

4.2.4 Direction

Given the importance of knowing the vessel direction a triple-axis accelerometer and magnetometer compass board model LSM303 (Figure 18) was selected to be part of the autonomous system. With this module is possible detecting magnetic north and use this as a

reference of navigation. It is also equipped with a classic 3-axis accelerometer that measures which direction is down towards the Earth by measuring gravity.
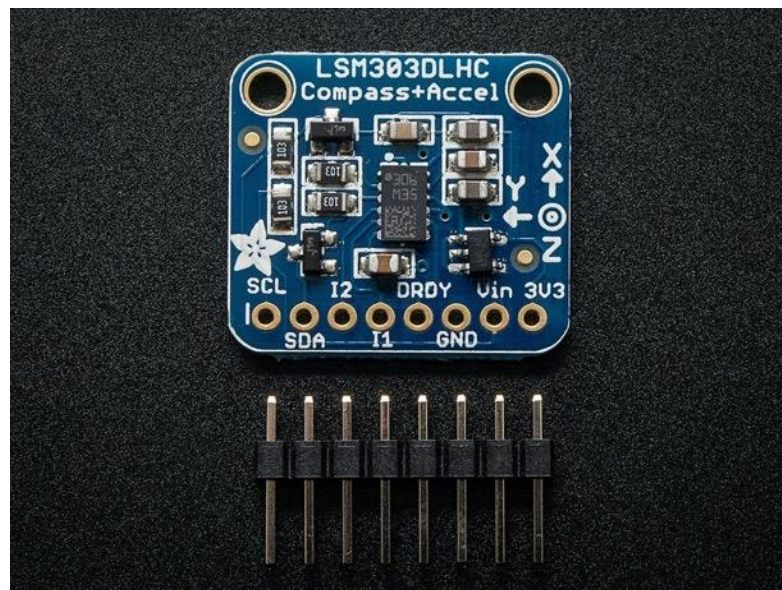
Figure 18 - LSM303 Compass module. Source: https://www.adafruit.com

4.2.5 Communication

To establish a communication link between the boat and land a LoRa 21U4 II module (Figure 19) was chosen. This device allows radio communication in 868MHz and achieving about 4km in Line of sight (LoS) condition. In addition it can be set using the Arduino's IDE or serial communication.

Figure 19 - LoRa32U4 II ATmega32U4 module. Source: https://www.usinainfo.com.br

4.2.6 Speed Controller

To adjust the speed of each thruster a controller was selected (Figure 20). It is a 15KHz model that allows DC voltage between 6 and 60V and currents from 0 to 30A. In addition, it can be set using a variable resistor with a third adjustable terminal, fitting what we need. Its display shows the instantaneous percentage of speed (compared with maximum).

Figure 20 - Speed Controller. Source: https://www.eletrodex.com.br

4.2.7 Battery

During the path-following simulations discussed in section 5 SYSTEM S, to maintain the speed around 1.5m/s the vessel needed a thrust force around 24 N. Based on the motor's experimental test results showed in Table 5 plot shown in Figure 21 was constructed, that gives us the relationship between the thrust force and the load current.
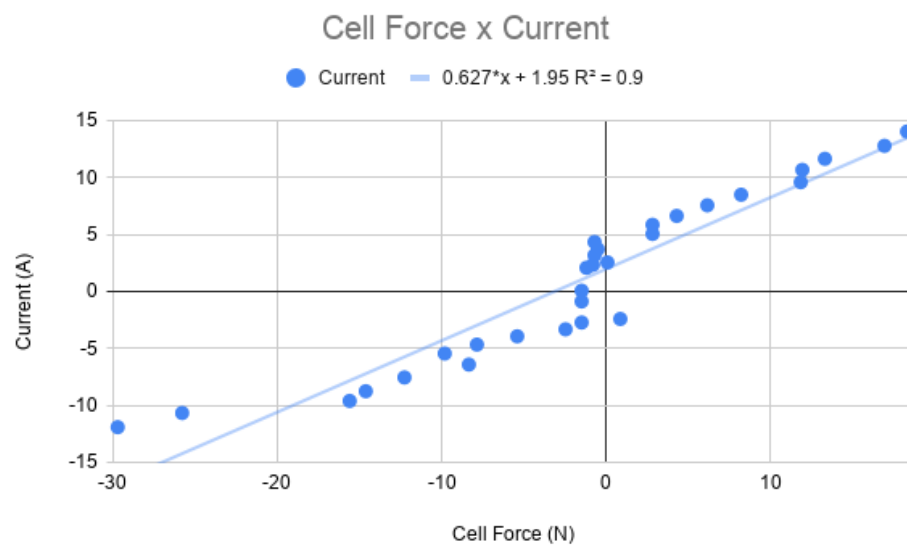
Figure 21 - Thrust Force versus Load Current. Based in Magalhães [15].

Using the linear approximation shown in Figure 21:

$$LoadCurrent = 0.627 * 24 + 1.95$$

$$LoadCurrent \cong 17.0 \ A$$

(10)

To simplify we can consider a linear relationship between the battery capacity and the load current. Also, considering the endurance of 6 hours defined on section 3.2 Operational Profile of the Vessel, thus:

$$BatteryCapacity = LoadCurrent * Time$$

$$BatteryCapacity = 17.0\ A * 6\ hours \tag{11}$$

$$BatteryCapacity = 102.0\ Ah$$

These results give us an idea about the battery size and based on that, a 120Ah marine battery model Navy-RME120 from the company Impact was selected. Figure 22

Figure 22 – Marine Battery. Source: https://produto.mercadolivre.com.br/MLB-837670199-bateria-impact-

nautica-navy-rme-120-120ah-motores-eletricos-_JM.

4.2.8 Hardware Architecture

In Figure 23 it is possible to observe the connections between each subsystem and its types of communication. With the GPIOs the system is able to send voltage signals to the Speed Controller and change the motor's speed. As explained by Zoss [18], UART or I^{2}C connections depends on the manufacturer for the device, however, it is common to see devices that allow rapid data access to elect to use I^{2}C, while those needing larger data single data streams use UART connections.
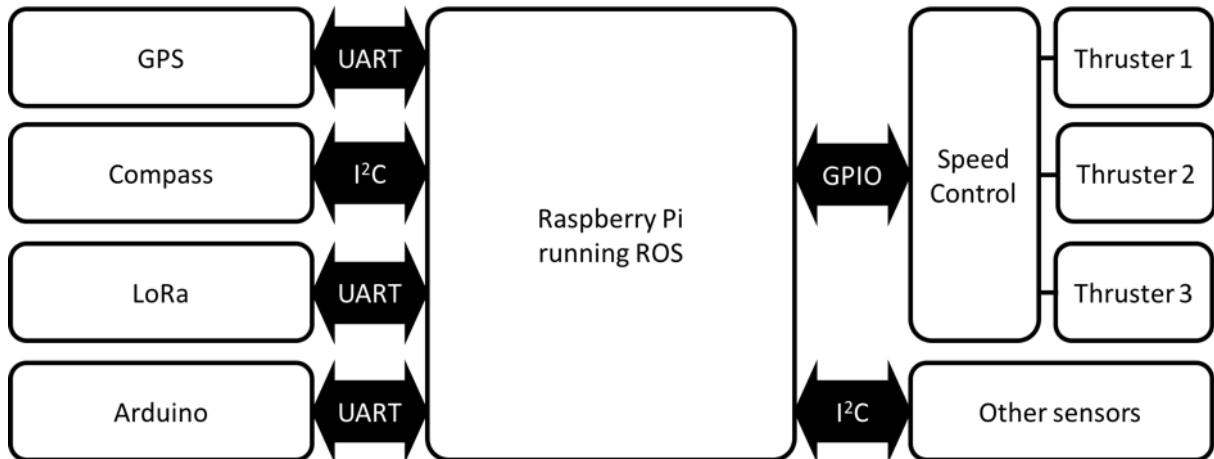
Figure 23 - Hardware architecture.

4.3 Software And Operational

The middleware used was the ROS (Robot Operating System), which is a flexible framework for writing robot software. Its structure is based on languages like C++, Python, Cmake, Ruby and Common Lisp. Basically, it is a collection of tools, libraries, and conventions that aim to simplify the task of creating complex and robust robot behavior across a wide variety of robotic platforms. The distribution adopted was the ROS Melodic (Figure 24), that matches with the Linux version of our system, an Ubuntu 18.04.3 LTS (codename bionic).
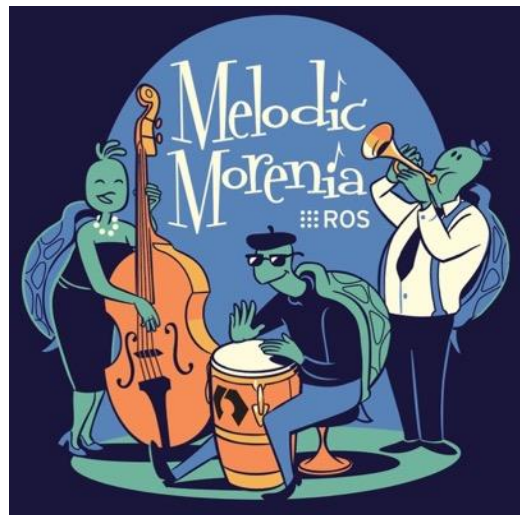
Figure 24 - ROS Distro Melodic. Source: http://wiki.ros.org

In ROS, each subsystem is written as a package (that can be written in Python or C++) that runs as a node. For instance, the system in Figure is running an autonomous boat with GPS, front-facing laser, and an IMU. Each of these sensors cited before has a package, ensuring modularity, reusability and easy implementation.

To simulate the present robot behavior a toolbox called Gazebo was used. It is a well-designed simulator that makes possible to rapidly test algorithms, design robots, perform tests, train AI system, etc. Gazebo offers the ability to accurately and efficiently simulate robots in outdoor environments. Basically, it is a robust physics engine, high-quality graphics, and convenient

programmatic and graphical interfaces. In addition, Gazebo is totally compatible with ROS and can save a lot of time and money when used in new projects.
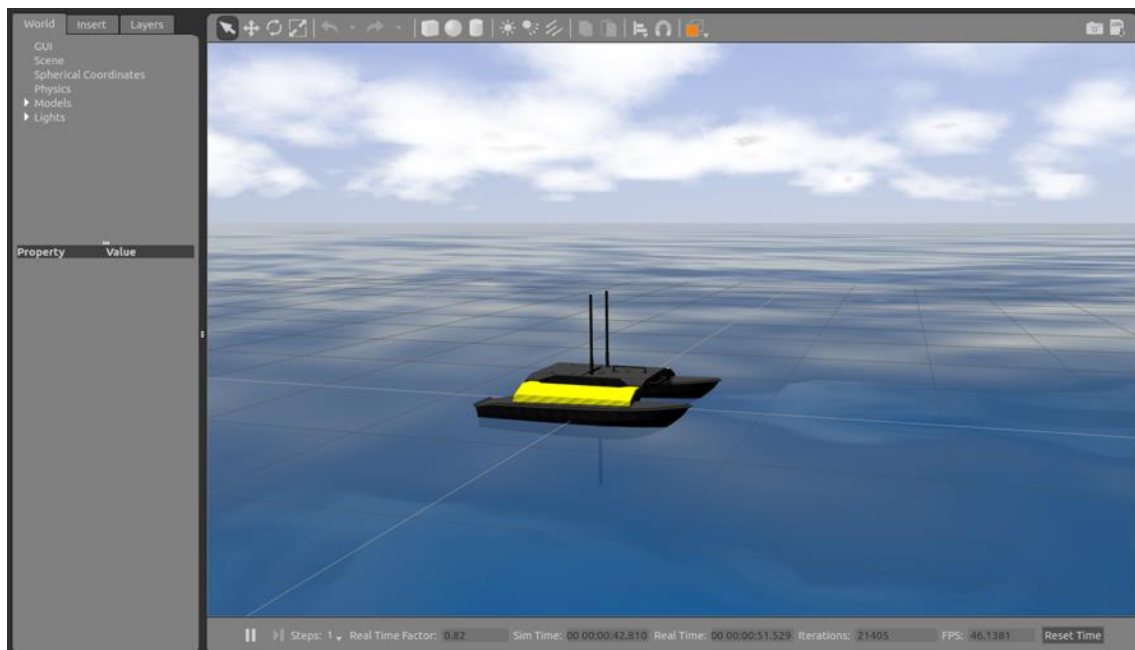
Figure 25 - Gazebo Simulator running the Heron USV software. Source: https://clearpathrobotics.com

Figure 25 shows the Heron USV running in the "Gazebo + ROS" environment and Figure 26 shows the same vessel physically built.

Figure 26 - Heron USV. Source: https://clearpathrobotics.com

The toolbox Gazebo has a huge options of packages developed by third parts and in these simulations some modules were used, for instance, the Maneuvering, Waves and Wind Model.

In this work, the Thrust Model had to be developed by the author due to its nonconventional arrangement.

4.3.1 Maneuvering Model

This model was implemented on Gazebo by Bingham [26] and uses the Nonlinear Maneuvering Model in Equation (12) from Fossen [21], expressed by:

$$M_{RB}\dot{v} + C_{RB}(v)v + M_A\dot{v}_r + C_A(v_r)v_r + D(v_r)v_r = \tau + \tau_{wind} + \tau_{waves} \tag{12}$$

Where,

M_{RB} − rigid body Interia Matrix
C_{RB} − rigid body Coriolis and centripetal Matrix
M_A − hydrodynamic Added Mass Matrix
C_A − Coriolis and centripetal Matrix for the added mass
D − hydrodynamic Damping Matrix
v − velocity vector $[u, v, r]^T$
v_r − relative velocity vector $[u_r, v_r, r]^T$
τ − vector of control inputs
τ_{wind} − vector of wind forces
τ_{waves} − vector of wave induced forces

Using this system ROS-Gazebo, the components of the rigid-body force are calculated via the Gazebo physics engine and the previous hydrodynamic forces are calculated using the plugin implementation. These six degrees of freedom maneuvering model use the following matrices of Added Mass (13), Coriolis (14) and Damping (15).

$$M_A = \begin{bmatrix} -X_{\dot{u}} & 0 & 0 & 0 & 0 & 0 \\ 0 & -Y_{\dot{v}} & 0 & 0 & 0 & 0 \\ 0 & 0 & 0.1 & 0 & 0 & 0 \\ 0 & 0 & 0 & 0.1 & 0 & 0 \\ 0 & 0 & 0 & 0 & 0.1 & 0 \\ 0 & 0 & 0 & 0 & 0 & -N_{\dot{r}} \end{bmatrix} \tag{13}$$

$$C_A(v_r) = \begin{bmatrix} 0 & 0 & 0 & 0 & 0 & -Y_{\dot{v}}v_r - Y_{\dot{r}}r \\ 0 & 0 & 0 & 0 & 0 & -X_{\dot{u}}u_r \\ 0 & 0 & 0 & 0 & 0 & 0 \\ 0 & 0 & 0 & 0 & 0 & 0 \\ 0 & 0 & 0 & 0 & 0 & 0 \\ 0 & 0 & 0 & -Y_{\dot{v}}v_r - Y_{\dot{r}}r & -X_{\dot{u}}u_r & 0 \end{bmatrix} \tag{14}$$

$$D(v_r) = \begin{bmatrix} X_u + X_{u|u|}|u| & 0 & 0 & 0 & 0 & 0 \\ 0 & Y_v + Y_{v|v|}|v| & 0 & 0 & 0 & 0 \\ 0 & 0 & Z_w & 0 & 0 & 0 \\ 0 & 0 & 0 & K_p & 0 & 0 \\ 0 & 0 & 0 & 0 & M_q & 0 \\ 0 & 0 & 0 & 0 & 0 & N_r + N_{r|r|}|r| \end{bmatrix} \tag{15}$$

Section 4.5 Hydrodynamic Coefficients describes how these coefficients (the hydrodynamic derivatives) were obtained and shows their nondimensional values according to the estimations.

4.3.2 Waves Model

The Waves Model is based on the Gerstner Waves with three components [27], where the Amplitude, Period and Direction of each component can be defined. The wave behavior on the simulation is determined by the deepwater dispersion. To calculate the influence of the wavefield on the vessel, a footprint of the hull is used as a base, where the hull is decomposed into a simple grid, with points at each corner of the vessel. These points are used to calculate the vertical displacement [26]. Values of height and period of waves will be given in the 5 SYSTEM S section.

4.3.3 Wind Model

The Wind Model implemented in this plugin is based on Fossen [20], allowing the influence of wind on the motion of the surface vessel. In this model, the wind velocity on the vessel (V_w) is considered to be a constant velocity and direction. This constant wind velocity is specified as a three-element vector that specifies the wind speed in the world-frame x, y and z coordinates with units of m/s, in this case, the z component was ignored.
The resulting forces (Equations (16) and (17)) and moments (Equation (18)) on the vessel are calculated based on the user-specified force/moment coefficients and the relative wind velocity.

$$X_{wind} = C_X V_{R_X} |V_{R_X}| \tag{16}$$

$$Y_{wind} = C_Y V_{R_Y} |V_{R_Y}| \tag{17}$$

$$N_{wind} = -2.0 C_N V_{R_X} |V_{R_Y}| \tag{18}$$

The coefficients c_X, c_Y and c_N used were the same as Sarda [28], with values of 0.50, 0.50 and 0.33 respectively. Figure 27 shows the lateral and frontal projected windage areas.

Figure 27 - Lateral (left) and frontal (right) projected areas.

Values of these coefficients will be given in the 5 SYSTEM S section.

4.3.4 Thrust Model

The Thrust Model used in this simulation was implemented based on the Vectored Propulsion, explained in section 4.1.3 Vectored Propulsion. To simulate the thruster behavior, the commands need to be mapped in order to send a thrust force to be applied in the vessel. In this work, a linear thruster map was used, where the values of the commands (varying from -1.0 to 1.0) are scaled linearly to the maximum and minimum thrust forces defined by the user. These axial forces are applied at a point vertically separated from the CG as specified by the user, resulting in a coupling between the thrust force and the vehicle motion.
In this work, based on Magalhães [15] results, the motors were limited to 2kgf in the forward and backward directions. Based on Table 6 and Table 7, the point vertically separated from the CG was -0.35m.

4.3.5 GPS Model

This model simulates a GNSS (Global Navigation Satellite System) receiver. It gives to the system messages with the position and altitude in WGS84 coordinates. This model is able to introduce an additive Gaussian noise added to the position. Based on Tonon [33] and Svatoň [34], the standard deviation additive Gaussian noise used was 1.3m. The GPS reading update rate is 65 Hertz.

4.3.6 IMU Model

This model simulates an IMU (Inertial Measurement Unit) sensor. It gives the system messages that mimic a simple Attitude and Heading Reference System (AHRS) using the (erroneous) rates and accelerations. This model is able to introduce an additive Gaussian noise added to the linear acceleration and angular velocity. Based on Česenek [35] and Tonon [33], the standard deviation additive Gaussian noises used were $0.01m/s^2$ and 0.1rad/s. The IMU reading update rate is 65 Hertz.

4.3.7 Filtering

To filter the data from the GPS and IMU a simple Exponentially Weighted Moving Average (EWMA, Equations (19) - (22)) filter is used for smoothing data readings. One of the advantages of this method is that it consumes significantly less memory and works faster. The smoothing constant used was $\propto = 0.03$.

$$F \ and \ R \ \equiv Filtered \ and \ Raw \ data \tag{19}$$

$$\propto \ \equiv \ smoothing \ constant \tag{20}$$

$$F_{t0} = \ R_{t0} \tag{21}$$

$$F_t = F_{t-1} * (1-\propto) \ + \ R_t * \propto \tag{22}$$

4.3.8 Code Architecture

In Figure 28 in possible to observe the connections between each model inside the ROS and Gazebo environment. In a rough way, the vessel is submitted to the external loads (waves and wind) that may affect the vessel position. These motions are captured by the sensors (GPS and IMU) and send to the navigation algorithm, which interprets the values and returns the results to the thrusters according to the situation.
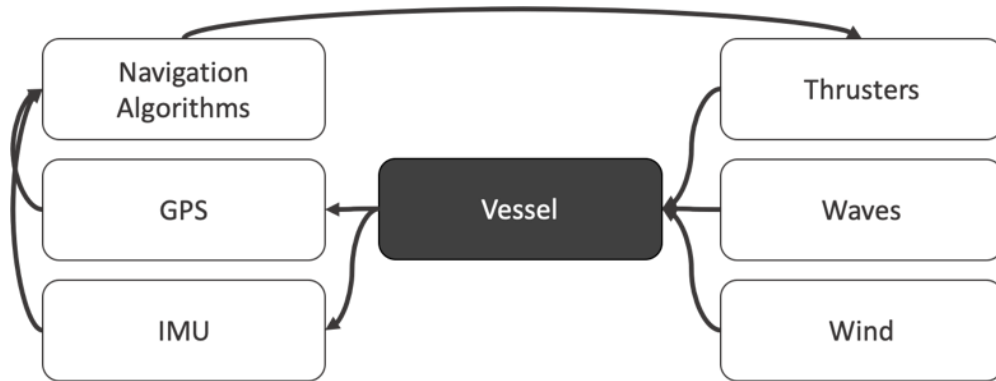
Figure 28 - Code architecture.

4.4 Control Systems

This subsection aims to describe the strategies of control used to guide the system during the accomplishment of its missions. Three navigation modes are discussed and explored.

4.4.1 Remote-Controlled

The remote-controlled mode is used in order to send commands to the system. In this mode, the operator will be able to arm/disarm the motors, set the speed ratios and send surge, sway and yaw commands.

4.4.2 Station-Keeping

This mode can be activated in two ways, based on the actual GPS position and heading of the vessel or by sending a new target-point (i.e. latitude, logintude and heading). The 3 meters accuracy of the GPS module will be used as a boundary to the station-keeping mode, so, if the distance between the setpoint and the vessel is less than this value nothing happens. However, if the distance error is greater than 10 meters the Path-following mode will be activated using an imaginary line (LOS - Line Of Sight strategy) connecting the actual position to the setpoint.

To handle the heading error, the boat will correct its orientation only if its value is greater than 1 degrees. The step-by-step of this mode of control is explained below:

1. Get/Receive GPS position and Compass heading.
2. If the heading error is greater than 1 degree:
   2.1. Uses a PID controller to estimate τ_c
   2.2. Calculate thrusters' output using the TA algorithm (subsection 4.1.3 Vectored Propulsion)
   2.3. Send the command to the motors
3. If the heading error is less than 1 degrees:
   3.1. Pass
4. If the distance error is greater than 5 meters and fewer than 20 meters:
   4.1. Uses a PID controller to estimate τ_c
   4.2. Calculate thrusters' output using the TA algorithm (subsection 4.1.3 Vectored Propulsion)
   4.3. Send the command to the motors
5. If the distance error is greater than 20 meters:
   5.1. Go into the Path-following mode
6. If the distance error is less than 5 meters:
   6.1. Correct the heading to the next waypoint

4.4.3 Path-Following

The path-following method will be a simple way-point guidance system. This kind of solution is showed in Pereira [19] and Fossen [20]. The main idea is set way-points where the vessel has to achieve in order to complete the mission.

To calculate the distances and orientation between two GPS-coordinate points the Haversine formulation will be used [22]. To go from a point to another, a LOS (Line Of Sight) controller will be implemented, computing the desired yaw angle (ψ_d) as follows [19].

$$\psi_d = \tan^{-1}\left(\frac{HE_d - HE_p}{HN_d - Hn_p}\right)$$

(23)

$$HE \equiv Haversine\ Easting$$
$$HN \equiv Haversine\ Northing$$
$$d, p \equiv desired, present$$

Subject to:

$$\left(HE_d - HE_p\right)^2 + \left(HN_d - Hn_p\right)^2 \leq \rho^2 \tag{24}$$

$$\rho \equiv Radius\ of\ acceptance$$

Here, a new Motor Speed Control approach is proposed. This formulation depends on the desired yaw angle $\psi_{d,n+1}$ in the way-point $(n+1)$ and the instantaneous error $E(t)$, i.e. the distance between the Setpoint (SP) and the Process Variable (PV). Thus, the desired speed is defined as follows.

$$V_d = V_s \left[1 - \text{sech}(E(t))\left(1 - \frac{1}{e^{\alpha\psi_{d,n+1}}}\right)\right]$$

$$\alpha = \left(\frac{\pi}{\pi - 1}\right) \tag{25}$$

$$E(t) = SP - PV$$

$$V_d \equiv Desired\ speed$$
$$V_s \equiv Service\ speed$$
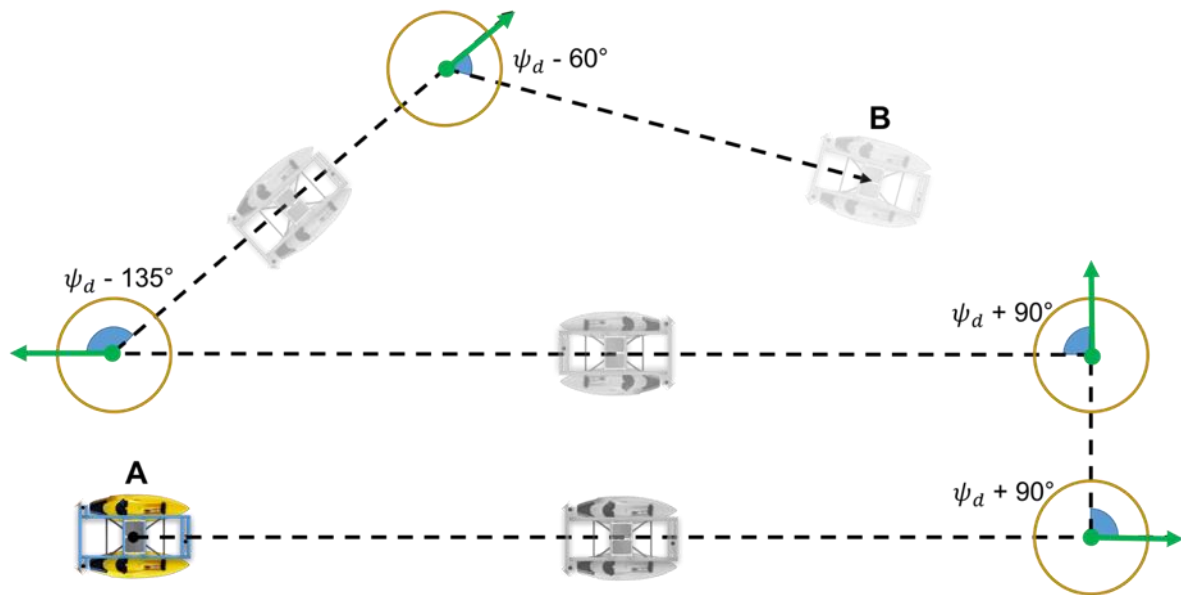
Figure 29 – Path-following trajectory example.

With the route defined (for instance, the way-points defined between A and B in Figure 29), a 3 steps algorithm is used as shown below:

1. The vessel navigates using V_d and ψ_d until the gold circles

2. Inside the gold circle:

   2.1. Navigates using V_d and $\psi_{d,n+1}$

3. When going out from the gold circle:

   3.1. Update n

4.5 Hydrodynamic Coefficients

In order to use the Maneuvering Model, the hydrodynamic maneuvering coefficients showed Table 8 are needed, and to do this some references were used to estimate the linear and non-linear coefficients.

Table 8 - Hydrodynamic coefficients used in the model.

Component	Comment
X_u	Axial Drag
$X_{u\|u\|}$	Axial Drag
Y_v	Crossflow Drag
$Y_{v\|v\|}$	Crossflow Drag
N_r	Crossflow Drag
$N_{r\|r\|}$	Crossflow Drag
$X_{\dot{u}}$	Added Mass
$Y_{\dot{v}}$	Added Mass
$Y_{\dot{r}}$	Added Mass
$N_{\dot{r}}$	Added Mass

4.5.1 Linear Hydrodynamic Coefficients

In order to estimate some linear hydrodynamic coefficients the equations developed by Inoue [29] were used, where the author estimated hull maneuvering forces based on physical considerations and model data. These nondimensional terms are given by Equation (26).

$$Y'_v = -(\frac{\pi}{2}\frac{T_{mid}}{L})(1 + \frac{2t_{stern}}{3T_{mid}})$$

$$N'_r = -[(0.54\frac{2T_{mid}}{L}) - (\frac{2T_{mid}}{L})^2](1 + 0.30\frac{t_{stern}}{T_{mid}})$$

(26)

Where,

$$T_{mid} \equiv draft\ at\ midship = \ 0.08m$$
$$t_{stern} \equiv trim\ at\ the\ stern = 0.00m$$
$$L \equiv ship\ length = 2.45\ m$$

4.5.2 Non-Linear Hydrodynamic Coefficients

Considering the damping, we have skin friction as the main component due to the boundary layers, and using known analytical methods is possible to calculate the needed hydrodynamic

coefficients.

Axial Drag

The vessel's surge drag can be represented by Equation (27), which can give us the non-linear axial drag coefficient shown in Equation (28).

$$R_{surge} = \frac{1}{2}\rho C_R A_w u|u| \tag{27}$$

$$X_{u|u|} = -\frac{1}{2}\rho C_R A_w \tag{28}$$

Where,
$$C_R \equiv resistance\ coefficient\ from\ the\ 1957\ ITTC = 0.08m$$
$$A_w \equiv total\ wetted\ surface\ area = 1.15m\ (each\ hull)$$

As we are using the quadratic axial drag coefficient $X_{u|u|}$ we will assume the linear X_u equal to zero.

Crossflow Drag

Here, the nondimensional terms were calculated using the Inoue [29] development, represented by Equations (29).

$$Y'_{v|v|} = (0.09 - 6.5(1 - C_b)\frac{T_{mid}}{B})$$

$$\tag{29}$$

$$N'_{r|r|} = -0.146 + 1.8\frac{C_b B}{L} - 6(\frac{C_b B}{L})^2$$

Where,
$$C_b \equiv block\ coefficient = 0.60$$
$$B \equiv breadth = 0.60m\ (each\ hull)$$

Added Mass

The added mass represents the mass of moving water when the body (in this case, the hull) accelerates.

Axial Added Mass

In order to estimate the axial added mass, the Blevis [32] analytical equations were used. In this case, the hull was considered as an ellipsoid, where the hull main dimensions were considered as the ellipsoid main axis dimensions.

$$X_{\dot{u}} = -\alpha \frac{4}{3} \rho \pi \left(\frac{L}{2}\right)\left(\frac{B}{2}\right)^2 \tag{30}$$

Where,

$\alpha \equiv empirical\ parameter\ measured\ by\ Blevins\ and$
$\quad determined\ by\ L/B, in\ this\ case\ \alpha = 0.0207$
$\rho \equiv water\ density = 1025\ kg/m^3$

Crossflow Added Mass

Here, the added mass was calculated using the strip theory. To do this, the hull was considered as a square plate with length equal to the draft at each point along the hull (x-axis). The equations used are based on Triantafyllou [31] works, that gives:

$$m_a = 4.754 \rho \alpha(x)^2 \tag{31}$$

Where,

$\alpha \equiv half\ the\ length\ of\ the\ square's\ side\ as\ a\ function\ of$
$\quad the\ axial\ position\ along\ the\ hull.$

Thus, to estimate the crossflow added mass, we have:

$$Y_{\dot{v}} = -\int_{stern}^{bow} m_a(x)dx$$

$$Y_{\dot{r}} = -\int_{stern}^{bow} x m_a(x)dx \tag{32}$$

$$N_{\dot{r}} = -\int_{stern}^{bow} x^2 m_a(x)dx$$

All these coefficients were calculated considering just one hull, however, our case is based on a catamaran vessel and because of this, all the coefficients were considered twice its original values, giving us a first-order approximation. After all the estimates, we have the results shown in Table 9.

Table 9 - Hydrodynamic coefficients estimated to the catamaran.

Component	Value
X_u	0.00
$X_{u|u|}$	-15.52
Y_v	-9.65

$Y_{v\|v\|}$	-47.74
N_r	-14.36
$N_{r\|r\|}$	-5.27
$X_{\dot{u}}$	-19.61
$Y_{\dot{v}}$	-25.92
$Y_{\dot{r}}$	-31.76
$N_{\dot{r}}$	-48.80

5 SYSTEM SIMULATIONS

This section aims to describe the way that simulations were carried out using all the previous information.

5.1 Case 1 setup – Checking a Ship's Loaded Draft Marks

This first case was simulated with some port conditions, more specifically, the Port of Tubarão, Vitória-ES, Brazil ones (Figure 30 and Figure 31). Information about the most frequent significant wave height (H_s), peak wave period (T_p) and the wind velocity (V_w) was found in Marquez [36]. This author gives us some data from each point shown in Figure 30, where our case is carried out inside the orange rectangle, close to the red circle "Pto n°: 2". The information about this point is shown in Table 10.
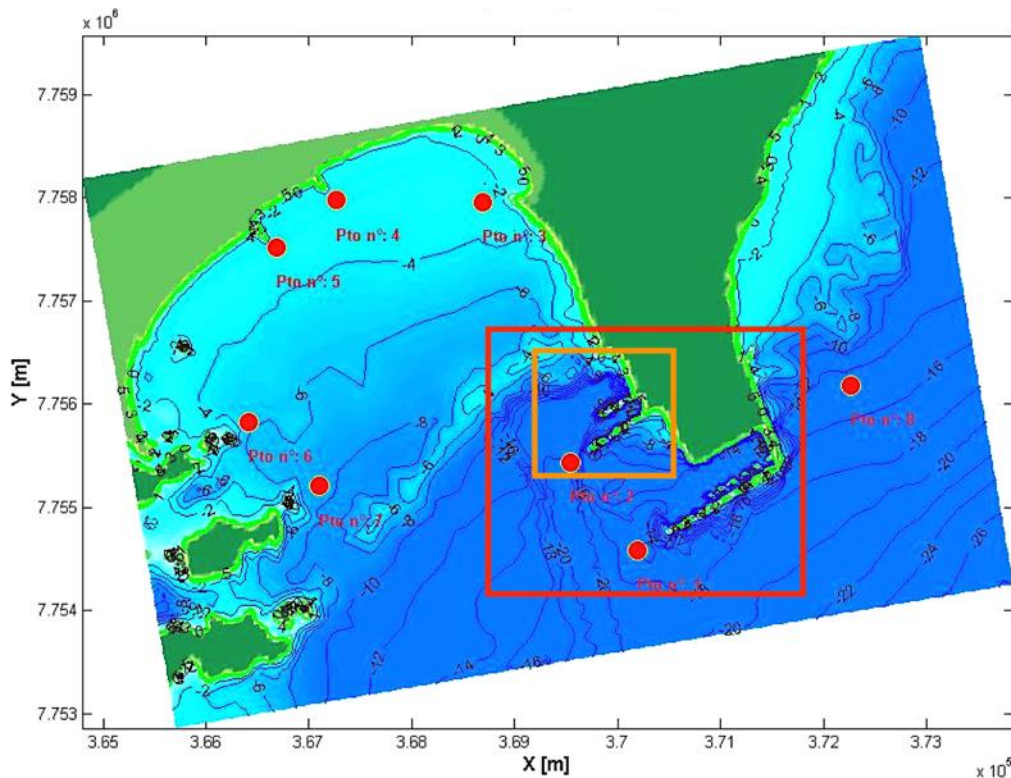
Figure 30 - Red circles are the points studied by Marquez [36]. Red rectangle is the Port of Tubarão location.

Orange rectangle is our scenario's case.

Figure 31 – Ore Vessels at the Port of Tubarão. Source: https://clickpetroleoegas.com.br/wp-content/uploads/2019/02/ArcellorMittal-abrirá-2-mil-vagas.jpg

Table 10 – Mean weather conditions by Marquez [36].

$H_s(m)$	$T_p(s)$	$V_w(m/s)$
0.26	1.94	1.93

In order to simulate the task of checking the ship's loaded draft marks, a path was planned as shown in Figure 32. The main idea here is simulating some different weather conditions following a path close to the ore vessel in the port, and we can imagine that the autonomous system is equipped with a visual system that captures the ship's loaded draft marks while the catamaran follows its path. The initial latitude and longitude point (0 inside the yellow circle in Figure 32) has coordinates (-20.29105558, -40.24375890). The waves and wind are applied perpendicular to the ship.
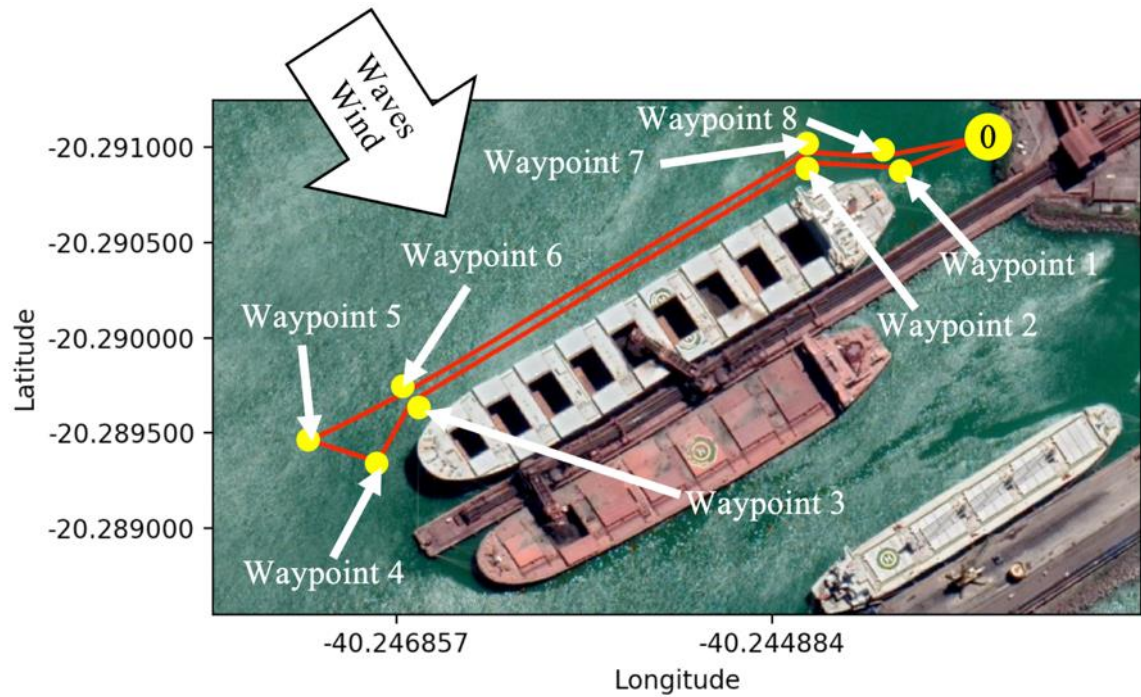
Figure 32 - Path planning (red line) to simulate the task of checking the ship's loaded draft marks. The yellow dots are the waypoints.

5.2 Case 2 setup - Verifying the Integrity of Anchoring Lines

This second case will be simulated with ocean conditions, more specifically, the Santos Basin, Santos-SP, Brazil ones (Figure 33). Information about the most frequent significant wave height (H_s), peak wave period (T_p) and the wind velocity (V_w) was found in Bouças [37], Ferreira [38] and Nascimento [39]. These authors give us some data from the basin shown in Figure 33, where our case is carried out. The information about the location is shown in Table 11.

Figure 33 – Santos Basin location.

Source:https://en.wikipedia.org/wiki/Santos_Basin#/media/File:Santos_basin_map.png.

Figure 34 – FPSO unit installed on the ocean. Source: https://petrobras.com.br/en/news/oil-and-natural-gas-output-in-february.htm.

Table 11 – Most frequent weather conditions by Bouças [37] and Ferreira [38].

$H_s(m)$	$T_p(s)$	$V_w(m/s)$
1.75	8.12	6.00

In order to simulate the task of verifying the integrity of the anchoring lines, a path was planned as shown in Figure 35. The main idea here is simulating some different weather conditions following a path close to the FPSO unit on the ocean, and we can imagine that the autonomous system is equipped with an auxiliary UUV (Unmanned Underwater Vehicle) that navigates below the water surface capturing images of the anchoring lines while the catamaran follows its path. The initial latitude and longitude point (0 inside the yellow circle in Figure 35) has coordinates (-25.39046196, -43.47434344). The waves and wind are applied perpendicular to the ship.
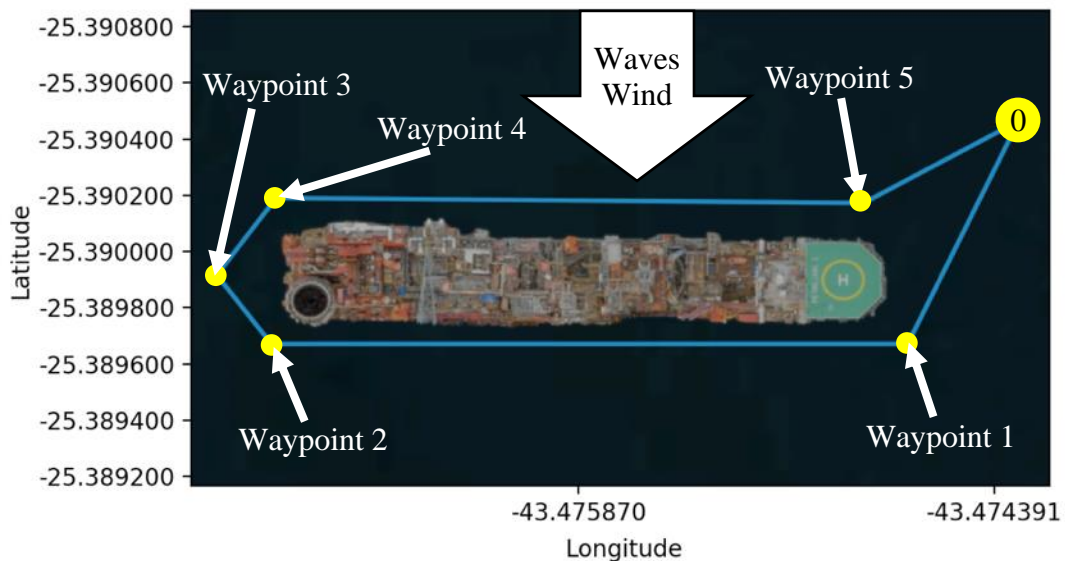
Figure 35 - Path planning (blue line) to simulate the task of verifying the integrity of the anchoring lines. The yellow dots are the waypoints.

5.3 CAD Models

In order to simulate the Autonomous System, a 3D model (shown in Figure 37 and Figure 36) was modeled with the main components (Hulls, Structural Beams, Electronic Boxes and Thrusters) described in the 4 section.
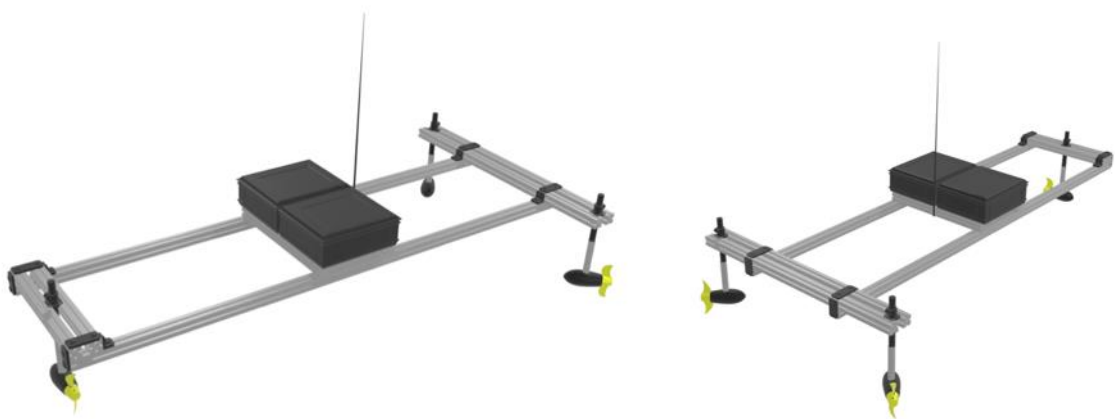
Figure 36 - 3D model of the Autonomous System.

Figure 37 - 3D model of the Autonomous System on the Kayaks.

In the simulation, the Ore Vessel and the FPSO unit were modeled as simple boxes with its main dimensions, shown in Table 12.

Table 12 - Ore Vessel and FPSO main dimensions.

Component	Lenght (m)	Breadth (m)
Ore Vessel	300.0	50.0
FPSO	214.0	38.0

The final results of these modeled scenarios can be observed in Figure 38 and Figure 39.
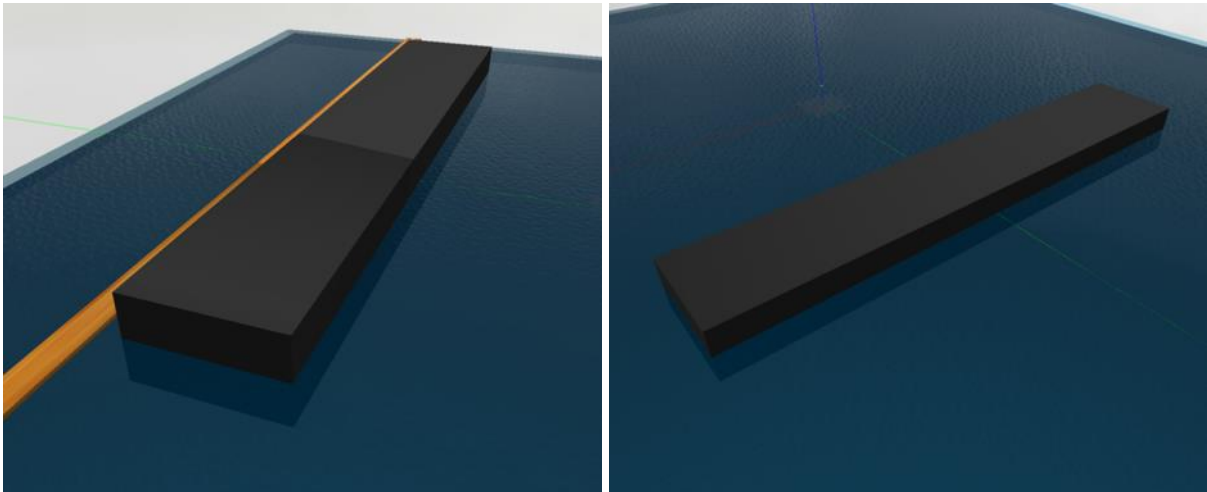
Figure 38 - Ore Vessel model in the Port (left) and FPSO unit (right) runing in the software Gazebo.
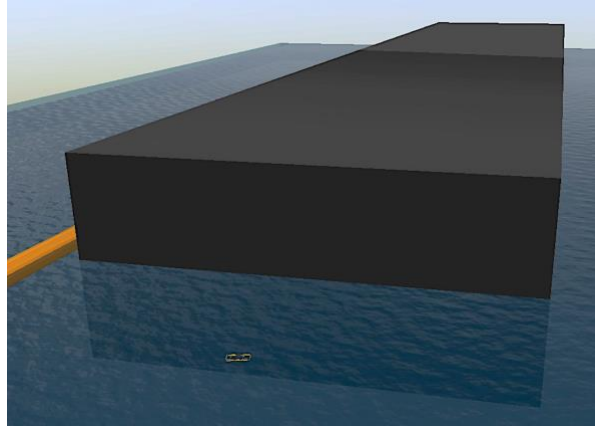
Figure 39 - Autonomous System runing besides the Ore Vessel in the software Gazebo.

5.4 Cases Simulation Matrix

To simulate all the autonomous system developed until this point at different weather conditions, a simulation matrix was built for each case in order to guide us through the simulations, where three main factors are changing: significant wave height (H_s) and peak wave period (T_p), wind velocity (V_w) and the maximum vessel velocity (V_s). The repetitions will be carried out considering the noise of the models of GPS, IMU and the initial conditions of the wave.

Case 1 – Checking a Ship's Loaded Draft Marks					
Port of Tubarão, Vitória - ES, Brazil					
Simulation	$H_s(m)$	$T_p(s)$	$V_w(m/s)$	$V_s(m/s)$	Repetitions
C1_1	-	-	-	0.75	3.00
C1_2	-	-	-	1.50	3.00
C1_3	0.26	1.94	-	0.75	3.00
C1_4	0.26	1.94	-	1.50	3.00
C1_5	0.26	1.94	1.93	0.75	3.00
C1_6	0.26	1.94	1.93	1.50	3.00
C1_7	-	-	1.93	0.75	3.00
C1_8	-	-	1.93	1.50	3.00

Case 2 – Verifying the Integrity of Anchoring Lines					
Santos Basin, Santos - SP, Brazil					
Simulation	$H_s(m)$	$T_p(s)$	$V_w(m/s)$	$V_s(m/s)$	Repetitions
C2_1	-	-	-	0.75	3.00
C2_2	-	-	-	1.50	3.00
C2_3	1.75	8.12	-	0.75	3.00
C2_4	1.75	8.12	-	1.50	3.00
C2_5	1.75	8.12	6.00	0.75	3.00
C2_6	1.75	8.12	6.00	1.50	3.00

C2_7	-	-	6.00	0.75	3.00
C2_8	-	-	6.00	1.50	3.00

5.5 Station-Keeping

This subsection aims to describe in which conditions the station-keeping capability of the system was simulated.

As showed in [40], the Dynamic Positioning capability numbers are based on numbers correlating with the Beaufort scale as illustrated in Table 13. Notice that in this case, the current speed was not considered once that we do not have this model in this work. Also, the DP capability number was limited from 0 to 3 (the original table has from 0 to 12) in order to have just an initial idea of the Station-Keeping performance.

Table 13 - DP capability numbers and Beaufort scale wind, wave height and wave period.

Beaufort number	DP capability number	Beaufort description	H_s (m)	T_p (s)	V_w (m/s)	C_s (m/s)
0	0	Calm	0.00	0.00	0.00	0.00
1	1	Light air	0.10	3.50	1.50	0.25
2	2	Litght breeze	0.40	4.50	3.40	0.50
3	3	Gentle breeze	0.80	5.50	5.40	0.75

Based on Table 13, the simulation matrix shown in Table 14 was built in order to test the system capabilities under different environmental conditions and headings.

Table 14 - Station-Keeping Simulation Matrix.

Simulation	Heading	Beaufort number	DP capability number	Beaufort description	H_s (m)	T_p (s)	V_w (m/s)
SK0_1	0	0	0	Calm	0.00	0.00	0.00
SK0_2	45	0	0	Calm	0.00	0.00	0.00
SK0_3	90	0	0	Calm	0.00	0.00	0.00
SK0_4	135	0	0	Calm	0.00	0.00	0.00
SK0_5	180	0	0	Calm	0.00	0.00	0.00
SK1_1	0	1	1	Light air	0.10	3.50	1.50
SK1_2	45	1	1	Light air	0.10	3.50	1.50
SK1_3	90	1	1	Light air	0.10	3.50	1.50
SK1_4	135	1	1	Light air	0.10	3.50	1.50
SK1_5	180	1	1	Light air	0.10	3.50	1.50
SK2_1	0	2	2	Litght breeze	0.40	4.50	3.40

SK2_2	45	2	2	Litght breeze	0.40	4.50	3.40
SK2_3	90	2	2	Litght breeze	0.40	4.50	3.40
SK2_4	135	2	2	Litght breeze	0.40	4.50	3.40
SK2_5	180	2	2	Litght breeze	0.40	4.50	3.40
SK3_1	0	3	3	Gentle breeze	0.80	5.50	5.40
SK3_2	45	3	3	Gentle breeze	0.80	5.50	5.40
SK3_3	90	3	3	Gentle breeze	0.80	5.50	5.40
SK3_4	135	3	3	Gentle breeze	0.80	5.50	5.40
SK3_5	180	3	3	Gentle breeze	0.80	5.50	5.40

Here, 0 degrees case means *following conditions*, 90 degrees means *beam conditions* and 180 degrees means *head conditions*.

6 RESULTS AND DISCUSSION

6.1 Case 1 results

6.1.1 Simulation C1_1

Considering that in this case there's no waves, wind and the maximum speed is low, the result was as expected. The adopted control of heading and motor speed demonstrated good behavior during the path-following (Figure 40).
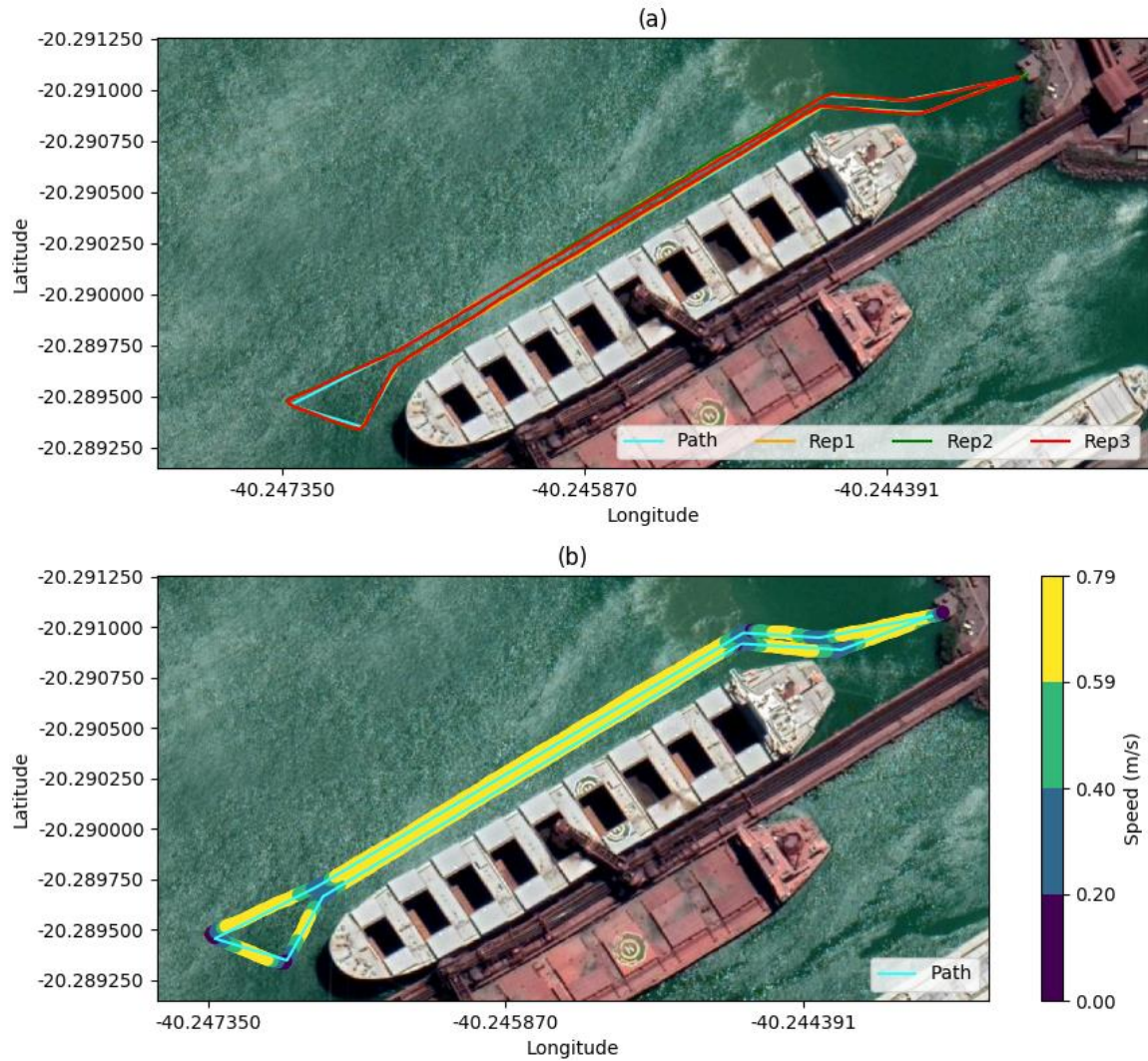
Figure 40 – Simulation C1_1 with the condition of no waves and no wind, a maximum speed of 0.75m/s. (a) System's path-following results for three repetitions. Basically the difference is the GPS output variation. (b) System's speed contour during Repetition 2, sometimes the value was greater than the limit due to the speed controller.

6.1.2 Simulation C1_2

Here the condition continues without waves and wind. However, the maximum speed is greater and due to this, the momentum acquired by the vessel makes it cross some waypoints and start the maneuvering later, as you can see in Figure 41.
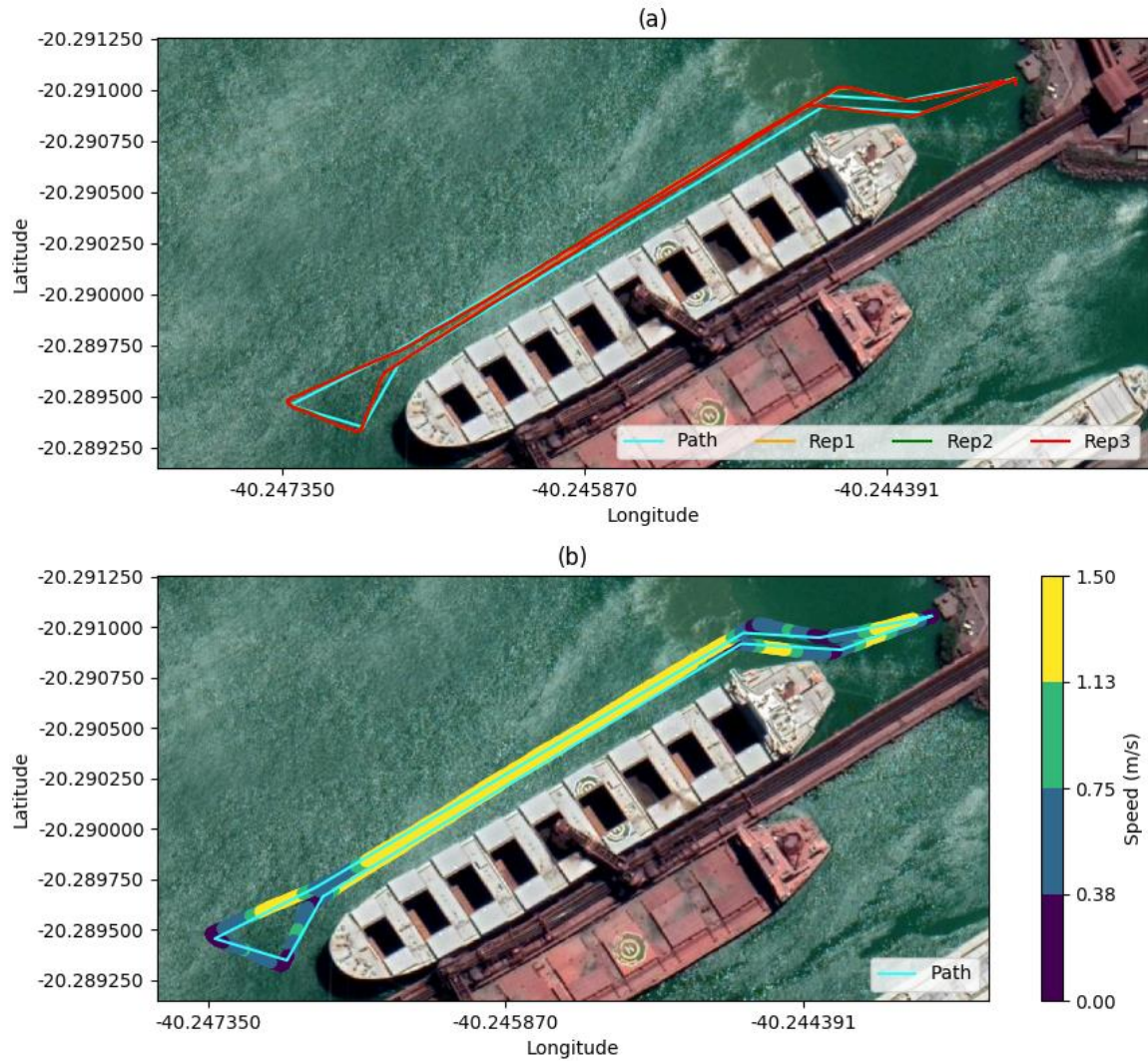
Figure 41 - Simulation C1_2 with the condition of no waves and no wind, a maximum speed of 1.50m/s. (a) System's path-following results for three repetitions. Basically the difference is the GPS output variation. (b) System's speed contour during Repetition 2.

6.1.3 Simulation C1_3

The condition here has no wind, but the effects of the waves are visible in Figure 42. During the longer paths the vessel drifted due to the waves and on the extreme left side of the path, during the heading correction meneuvering is possible to notice that the vessel has a low speed and the waves forced it to turn in the counterclockwise direction.
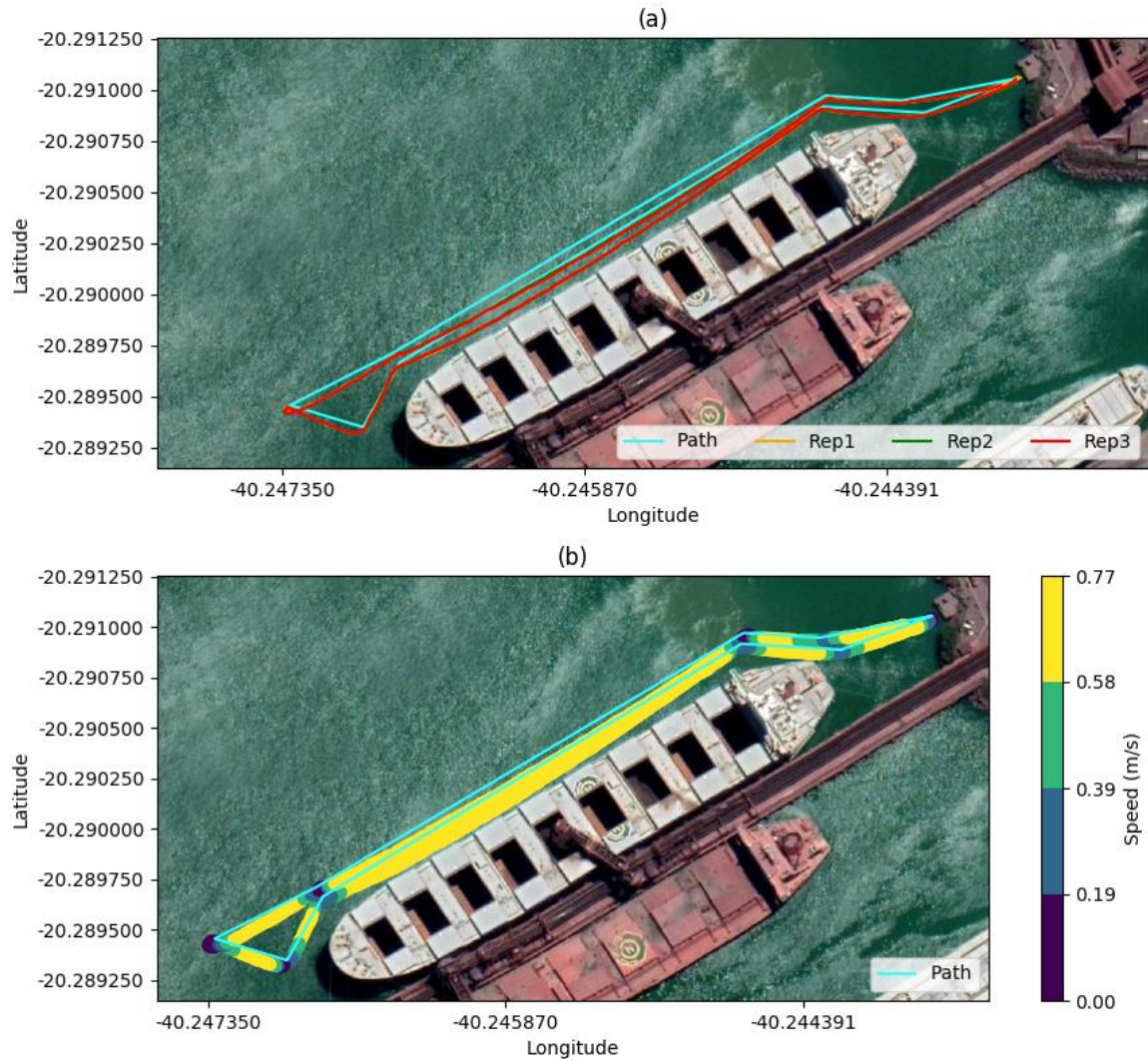
Figure 42 - Simulation C1_3 with wave height 0.26m and peak wave period 1.94s, no wind, a maximum speed of 0.75m/s. (a) System's path-following results for three repetitions. Basically the difference is the GPS output variation. (b) System's speed contour during Repetition 2, sometimes the value was greater than the limit due to the speed controller.

6.1.4 Simulation C1_4

Here there's kind of a mix between the simulations C1_2 and C1_3. In Figure 43 is possible to observe the momentum effect due to the speed and also the wave drift effect. This later with less apparent effect and this occurs because of the greater speed. The turning effect is also present on the extreme left-side path.
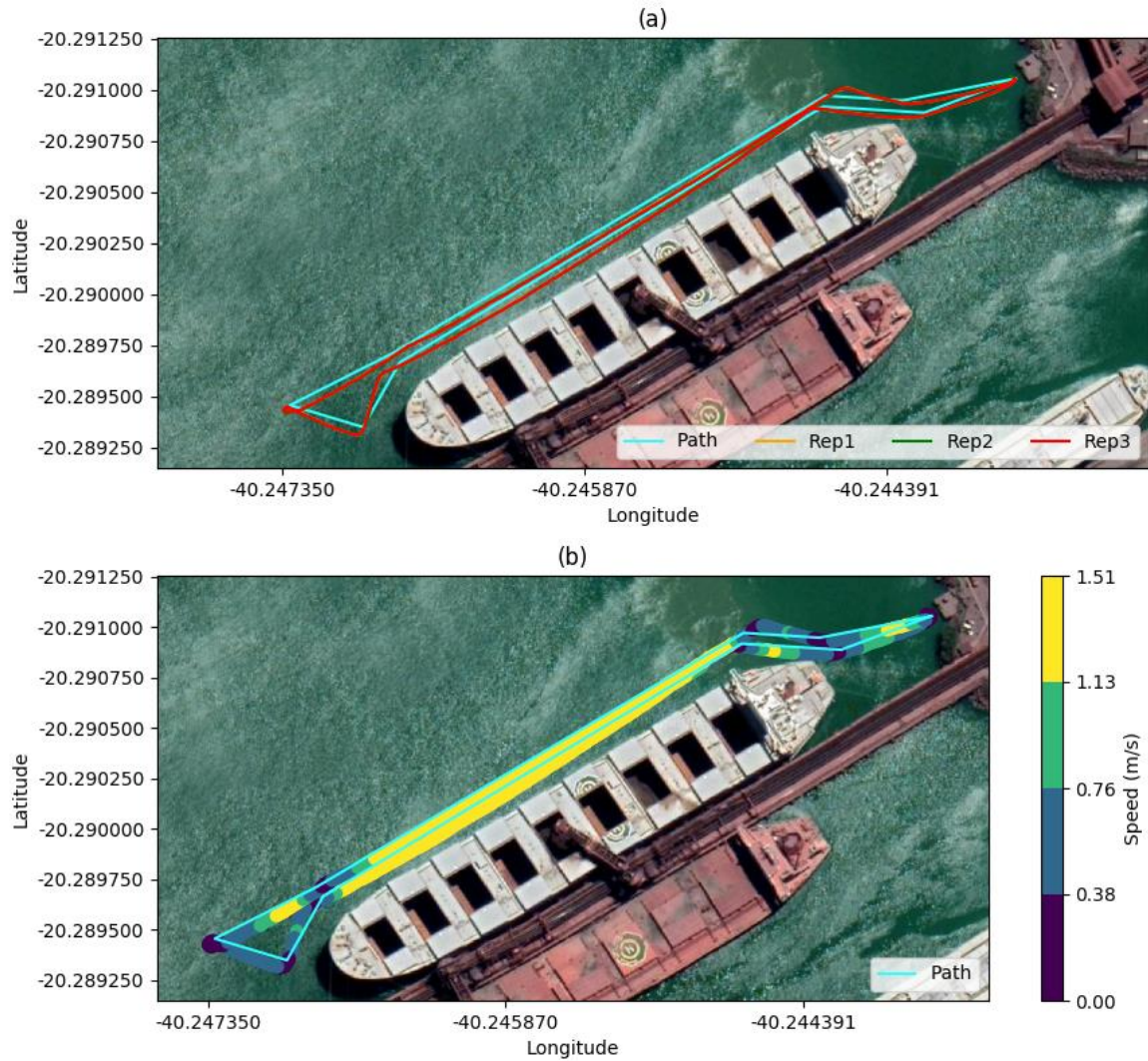
Figure 43 - Simulation C1_4 with wave height 0.26m and peak wave period 1.94s, no wind, a maximum speed of 1.50m/s. (a) System's path-following results for three repetitions. Basically the difference is the GPS output variation. (b) System's speed contour during Repetition 2.

6.1.5 Simulation C1_5

Here there's a full condition simulation with waves and wind. Comparing with the simulation C1_3, the drift effect was clearly increased by the constant wind force in Figure 44. The turning effect is also present on the extreme left-side path.
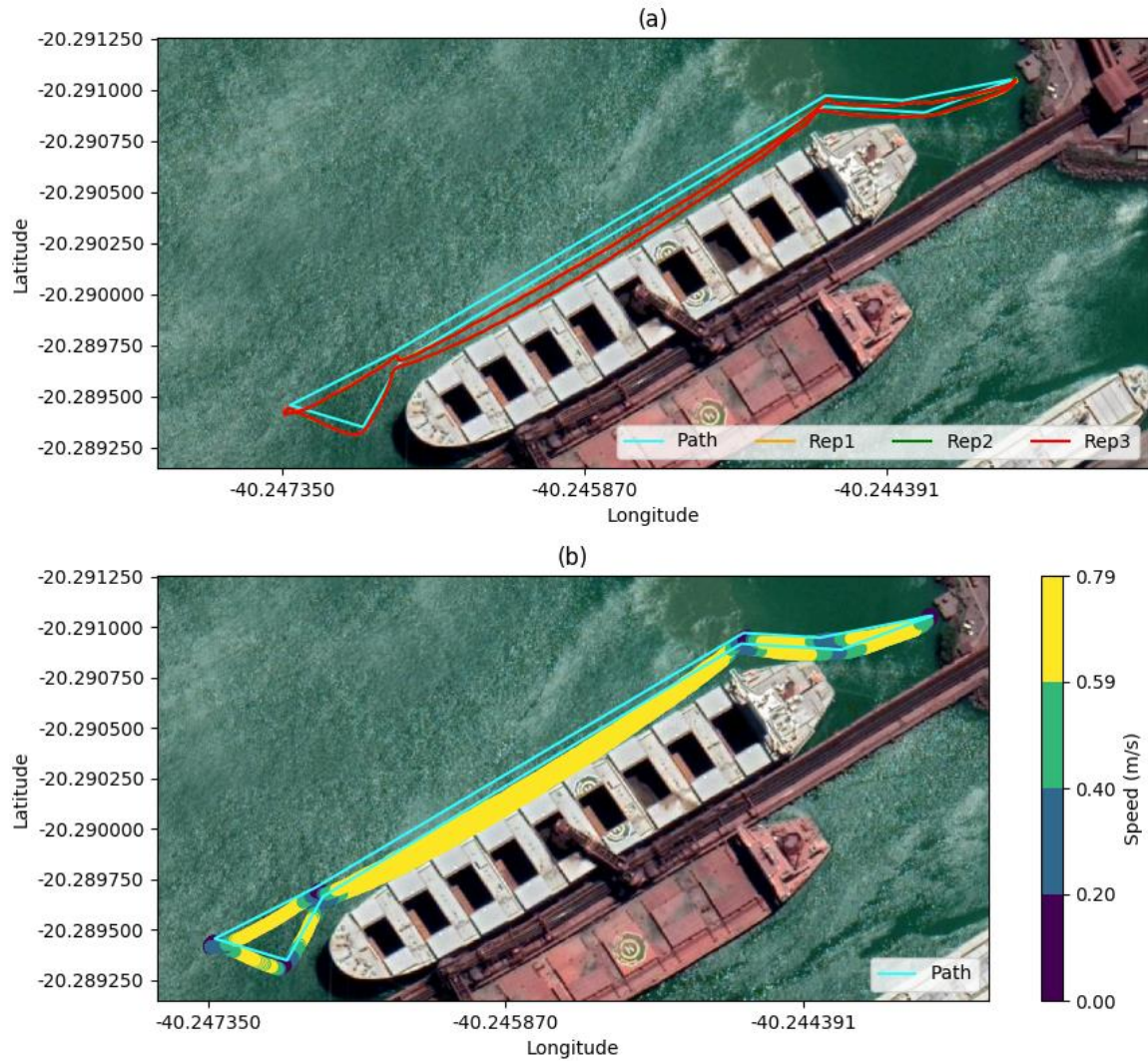
Figure 44 - Simulation C1_5 with wave height 0.26m and peak wave period 1.94s, wind speed of 1.93m/s and a maximum speed of 0.75m/s. (a) System's path-following results for three repetitions. Basically the difference is the GPS output variation. (b) System's speed contour during Repetition 2, sometimes the value was greater than the limit due to the speed controller.

6.1.6 Simulation C1_6

Here there's a full condition simulation with waves and wind. Figure 45 shows that probably the momentum effect in addition to the waves and wind caused some kind of instability and the vessel "collided" with the ship.
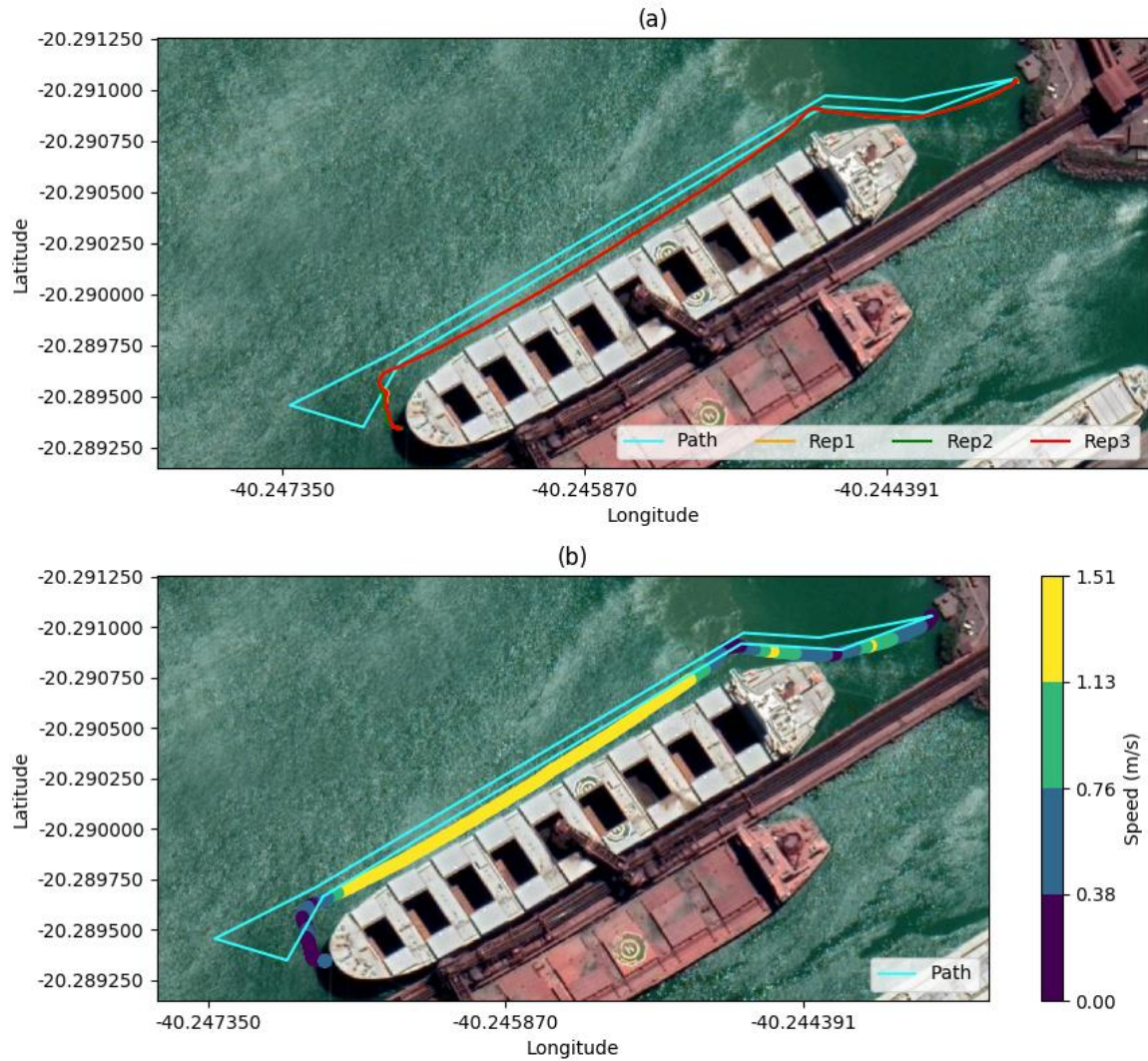
Figure 45 - Simulation C1_6 with wave height 0.26m and peak wave period 1.94s, wind speed of 1.93m/s and a maximum speed of 1.50m/s. (a) System's path-following results for three repetitions. Basically the difference is the GPS output variation. (b) System's speed contour during Repetition 2.

6.1.7 Simulation C1_7

Here there's just wind and the vessel at a lower speed. Figure 46 shows that these conditions are less intense than the waves one showed in Figure 42 from simulation C1_3. The turning effect also disappeared, which confirms that these forces and moments involved are weaker.
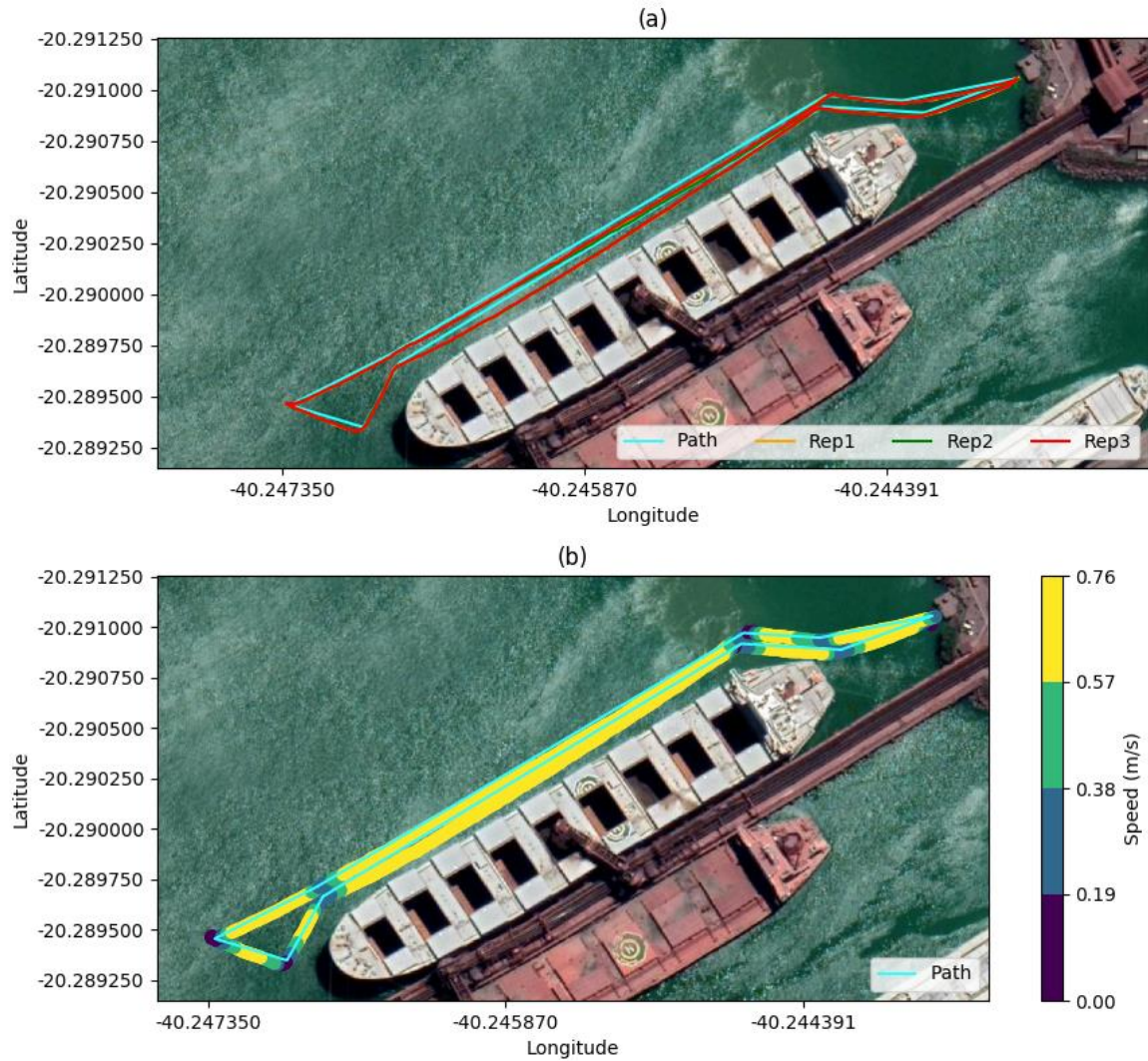
Figure 46 - Simulation C1_7 without waves, wind speed of 1.93m/s and a maximum speed of 0.75m/s. (a) System's path-following results for three repetitions. Basically the difference is the GPS output variation. (b) System's speed contour during Repetition 2.

6.1.8 Simulation C1_8

Here there's just wind and the vessel at a lower speed. Figure 47 seems a mix between the simulation C1_2 and C1_7 due to the momentum effect that reduces the deviation of the longer paths but increases the waypoint turn maneuvering. The turning effect also disappeared in this condition.
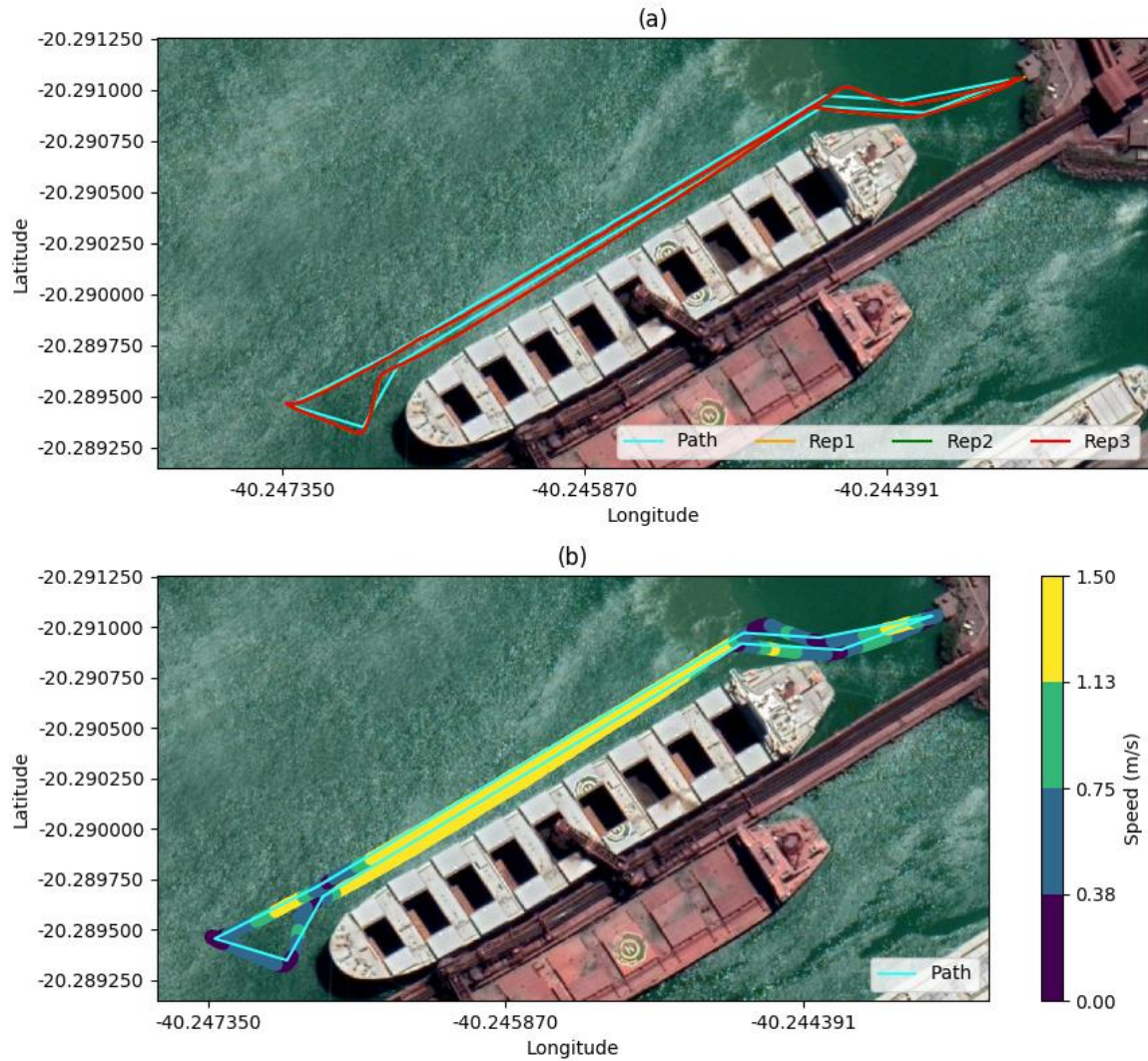
Figure 47 - Simulation C1_8 without waves, wind speed of 1.93m/s and a maximum speed of 1.50m/s. (a) System's path-following results for three repetitions. Basically the difference is the GPS output variation. (b) System's speed contour during Repetition 2.

6.2 Case 2 results

6.2.1 Simulation C2_1

Similarly to the simulation C1_1, this case there's no waves, wind and the maximum speed is low, so, the result was as expected. The adopted control of heading and motor speed demonstrated good behavior during the path-following (Figure 48).
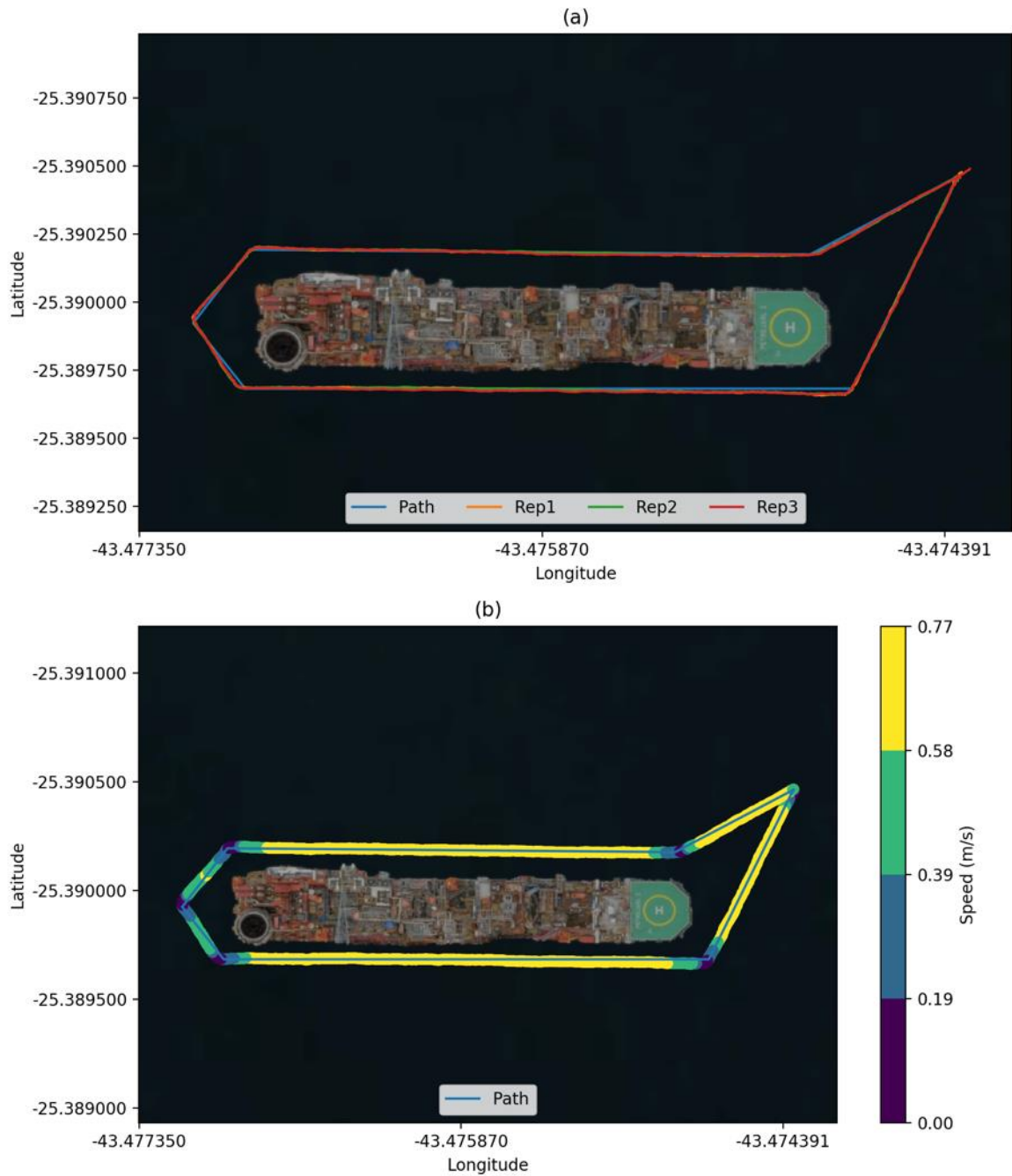
Figure 48 - Simulation C2_1 with the condition of no waves and no wind, a maximum speed of 0.75m/s. (a) System's path-following results for three repetitions. Basically the difference is the GPS output variation. (b) System's speed contour during Repetition 2, sometimes the value was greater than the limit due to the speed controller.

6.2.2 Simulation C2_2

Here the condition continues without waves and wind. However, as in Case 1, the maximum speed is greater and due to this, the momentum acquired by the vessel makes it cross some waypoints and start the maneuvering later, as you can see in Figure 49.
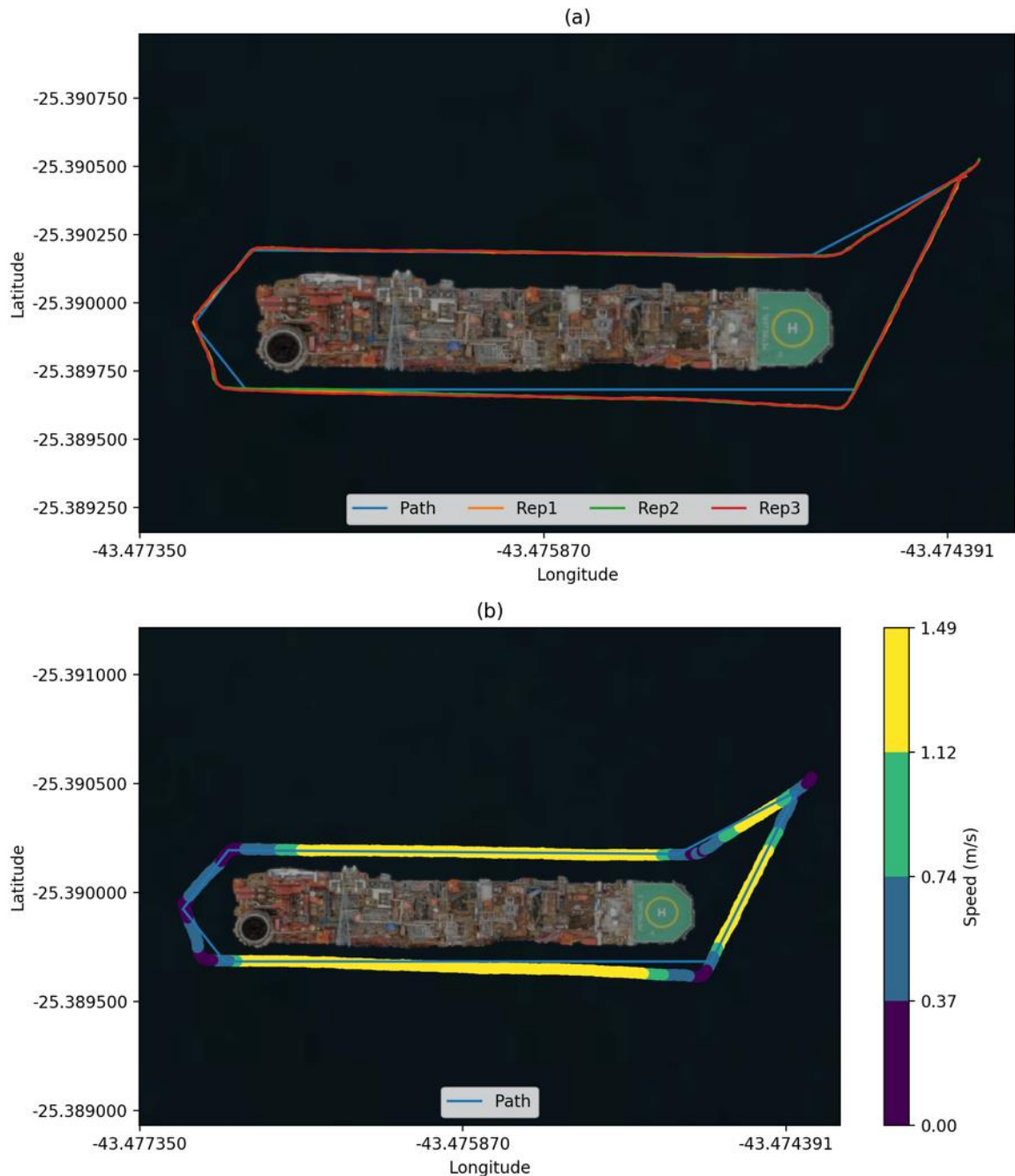
Figure 49 - Simulation C2_2 with the condition of no waves and no wind, a maximum speed of 1.50m/s. (a) System's path-following results for three repetitions. Basically the difference is the GPS output variation. (b) System's speed contour during Repetition 2.

6.2.3 Simulation C2_3

The condition here has no wind, but the effects of the waves are visible in Figure 50. During the longer paths and in some waypoints the vessel drifted due to the waves and as in the Case 1 simulation, on the extreme left side of the path, during the heading correction meneuvering is possible to notice that the vessel has a low speed and the waves forced it to turn in the counterclockwise direction. This turn has a bigger "radius" than in Case 1 and this may be correlated to the different wave conditions.
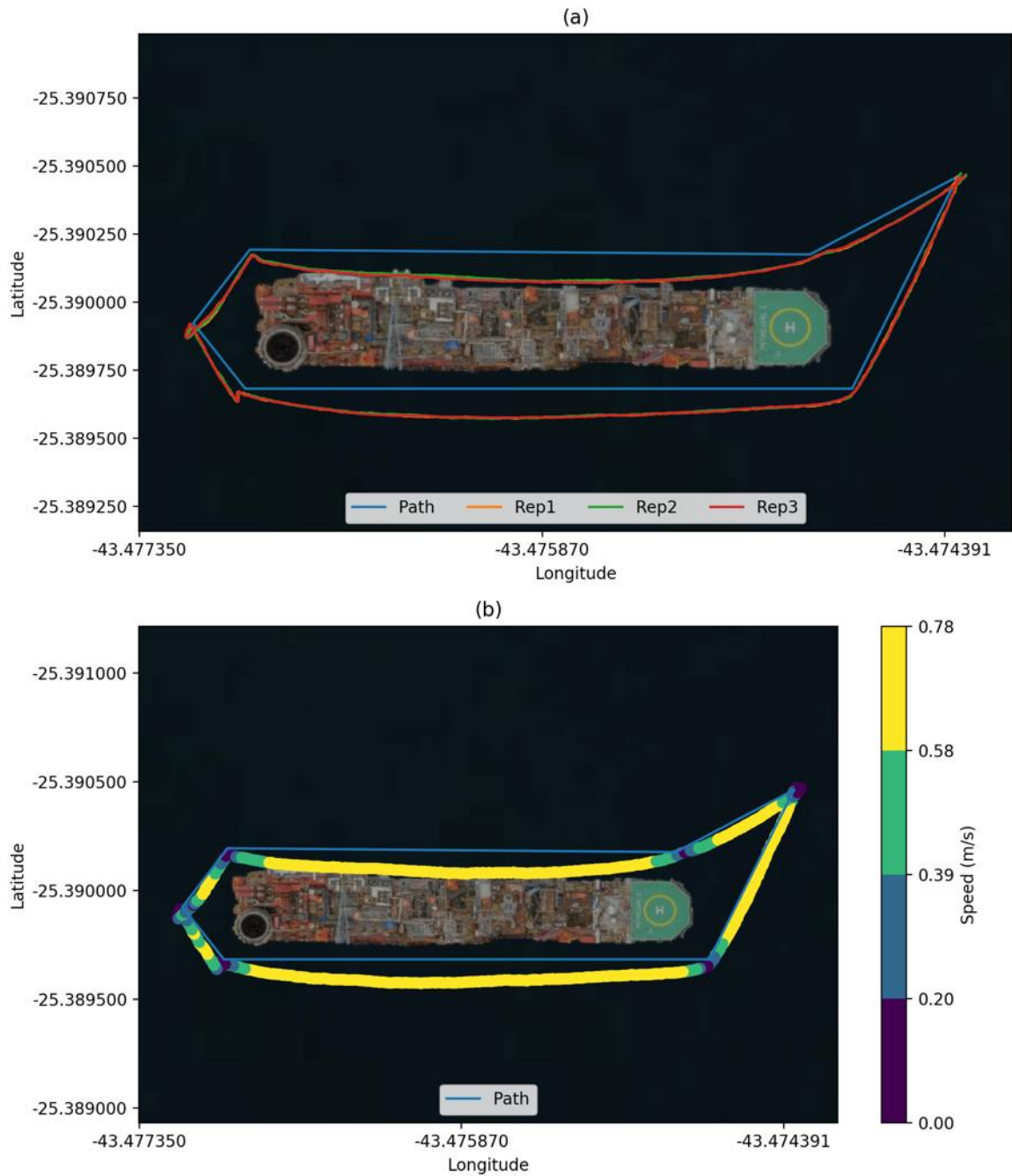
Figure 50 - Simulation C2_3 with wave height 1.75m and peak wave period 8.12s, no wind, a maximum speed of 0.75m/s. (a) System's path-following results for three repetitions. Basically the difference is the GPS output variation. (b) System's speed contour during Repetition 2, sometimes the value was greater than the limit due to the speed controller.

6.2.4 Simulation C2_4

Like in Case 1, this case seems a mix between the simulations C2_2 and C2_3. In Figure 51 is possible to observe the momentum effect due to the speed and also the wave drift effect. This later with less apparent effect and this occurs because of the greater speed. The turning effect is also present on the extreme left-side path.
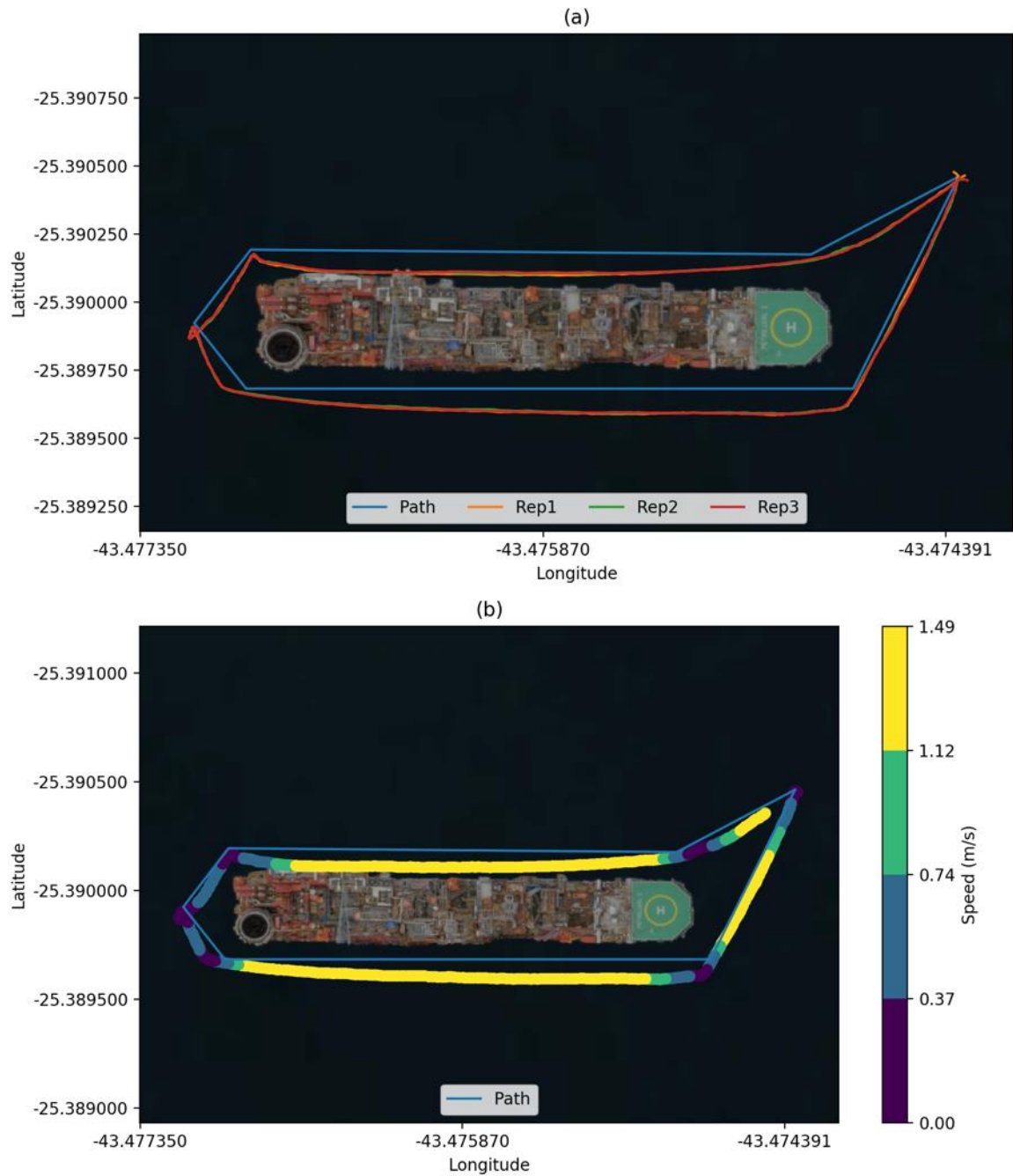
Figure 51 - Simulation C2_4 with wave height 1.75m and peak wave period 8.12s, no wind, a maximum speed of 1.50m/s. (a) System's path-following results for three repetitions. Basically the difference is the GPS output variation. (b) System's speed contour during Repetition 2.

6.2.5 Simulation C2_5

In the full condition simulation with waves and wind, the vessel can't go against the environment inside the waypoint 3 because according to the strategy adopted it's a point of low speed. Comparing with the simulation C2_3, the drift effect was clearly increased by the constant wind force in Figure 52.
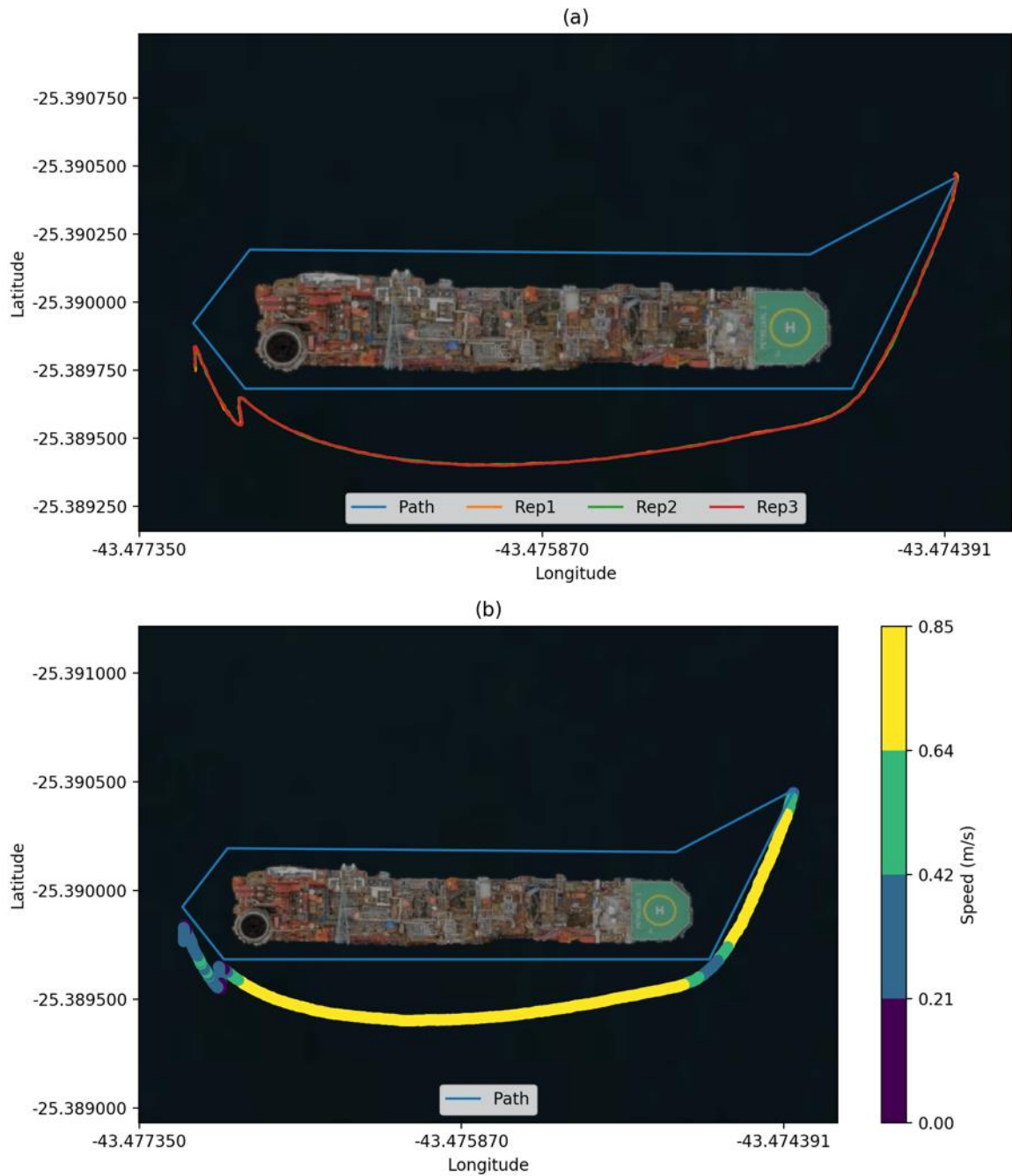
Figure 52 - Simulation C2_5 with wave height 1.75m and peak wave period 8.12s, wind speed of 6.00m/s and a maximum speed of 0.75m/s. (a) System's path-following results for three repetitions. Basically the difference is the GPS output variation. (b) System's speed contour during Repetition 2, sometimes the value was greater than the limit due to the speed controller.

6.2.6 Simulation C2_6

Figure 53 shows that the speed greater outside the gold circles didn't help the vessel against the environmental conditions.
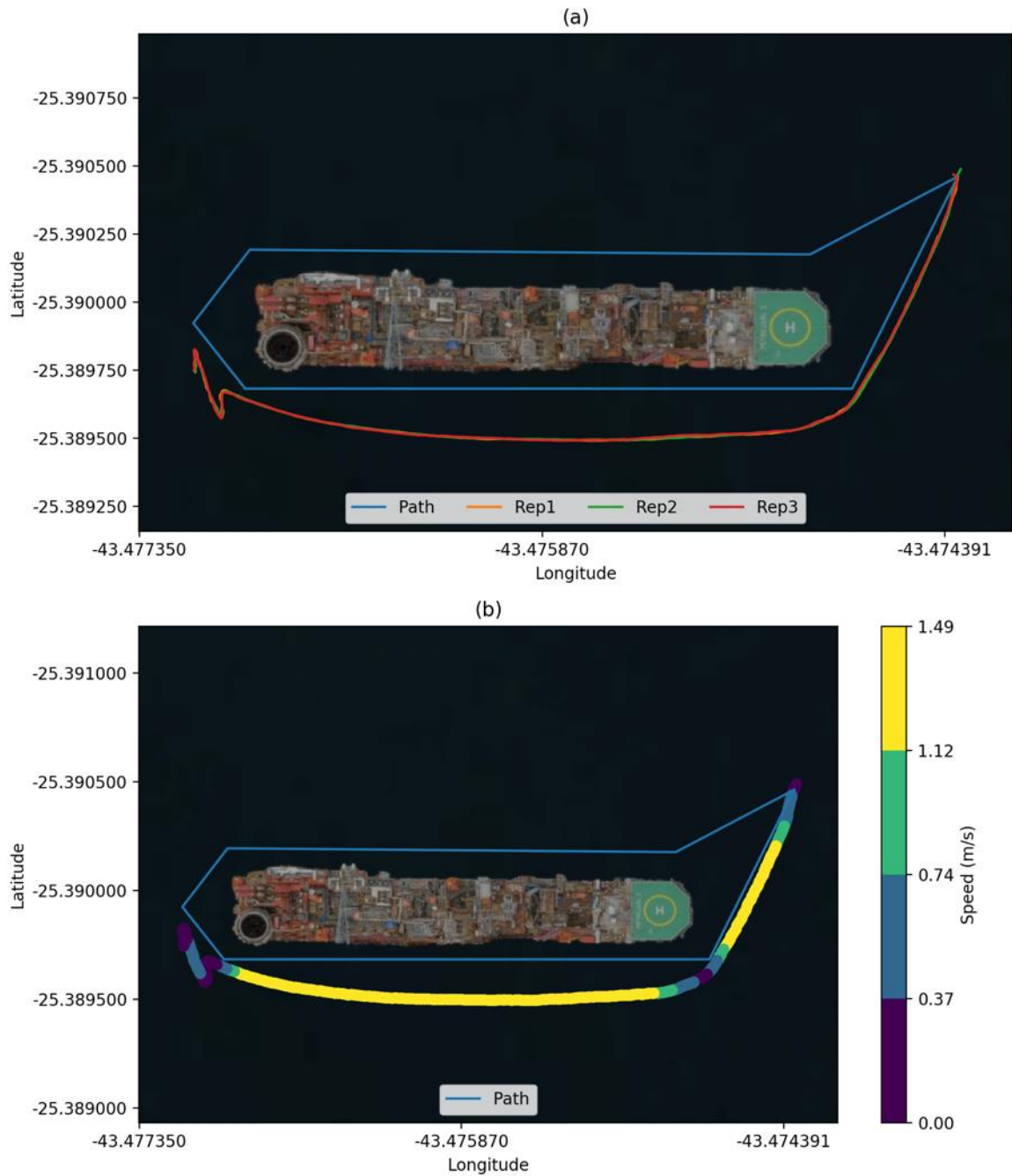
Figure 53 - Simulation C2_6 with wave height 1.75m and peak wave period 8.12s, wind speed of 6.00m/s and a maximum speed of 1.50m/s. (a) System's path-following results for three repetitions. Basically the difference is the GPS output variation. (b) System's speed contour during Repetition 2.

6.2.7 Simulation C2_7

Even in the only wind condition, the vessel didn't cross the waypoint 3 due to the constant wind force in a low-speed area. Figure 54 shows that the wind conditions are more intense than the waves one showed in Figure 50 from simulation C2_3.
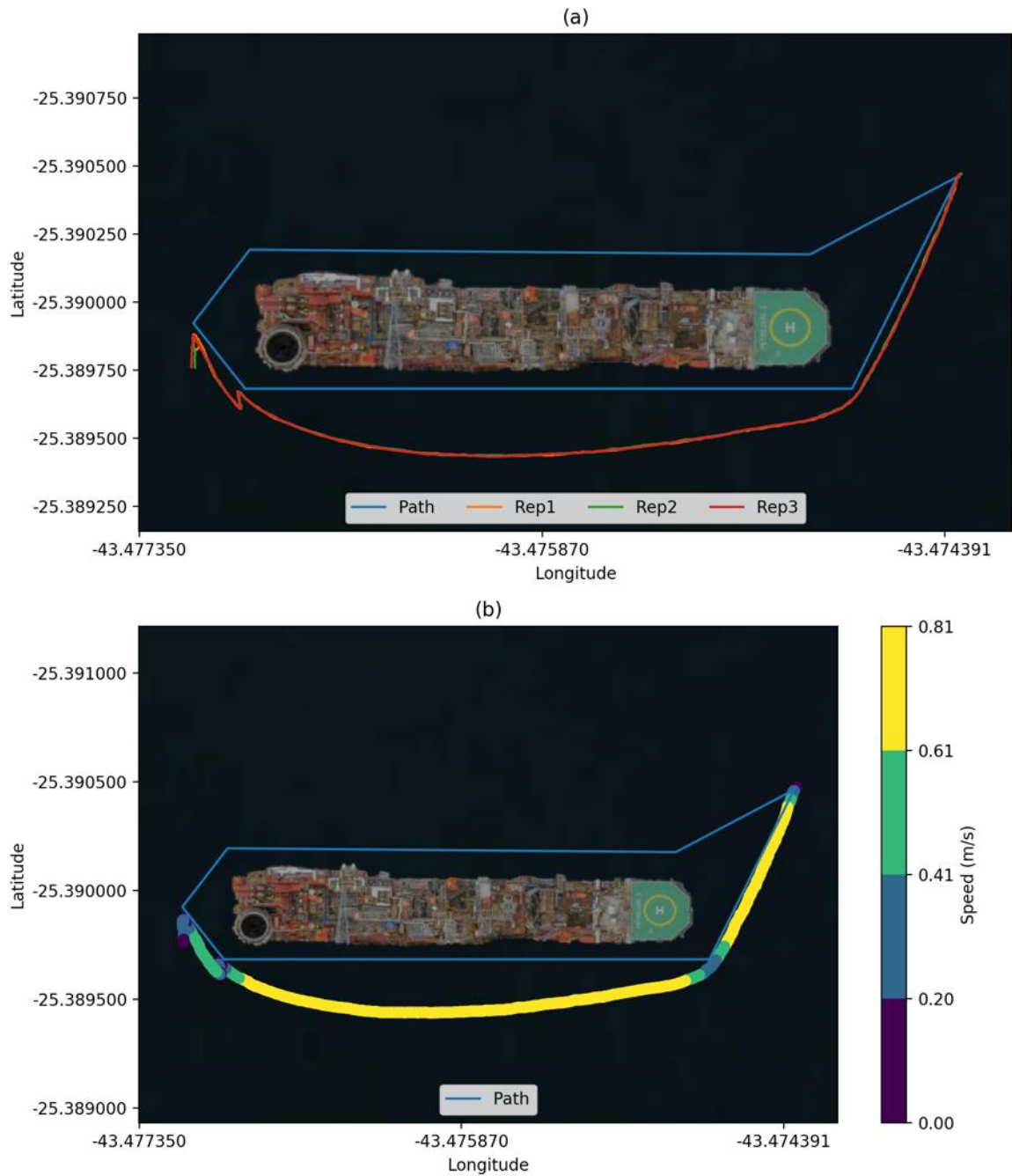
Figure 54 - Simulation C2_7 without waves, wind speed of 6.00m/s and a maximum speed of 0.75m/s. (a) System's path-following results for three repetitions. Basically the difference is the GPS output variation. (b) System's speed contour during Repetition 2, sometimes the value was greater than the limit due to the speed controller.

6.2.8 Simulation C2_8

Similarly to the previous simulation, the vessel didn't advance through the waypoint 3.
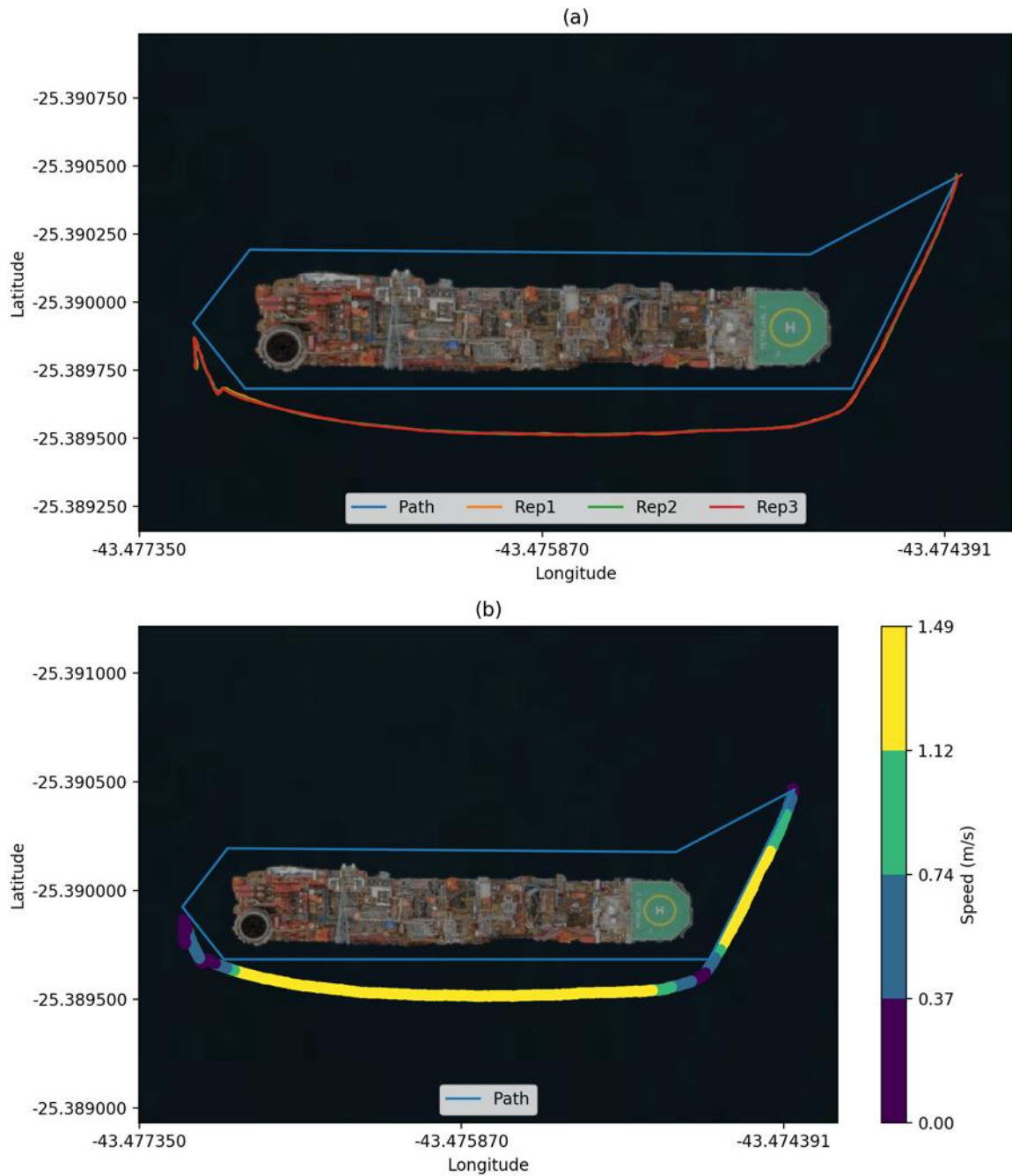
Figure 55 - Simulation C2_8 without waves, wind speed of 6.00m/s and a maximum speed of 1.50m/s. (a) System's path-following results for three repetitions. Basically the difference is the GPS output variation. (b) System's speed contour during Repetition 2.

6.3 Station-Keeping

As illustrated in Figure 56, the following results will have two limits that can be noticed in the plots from the simulations. The heading limit represents the maximum aperture of the yaw angle during the simulation and inside the position limits, we will have the path followed by the vessel during the time.
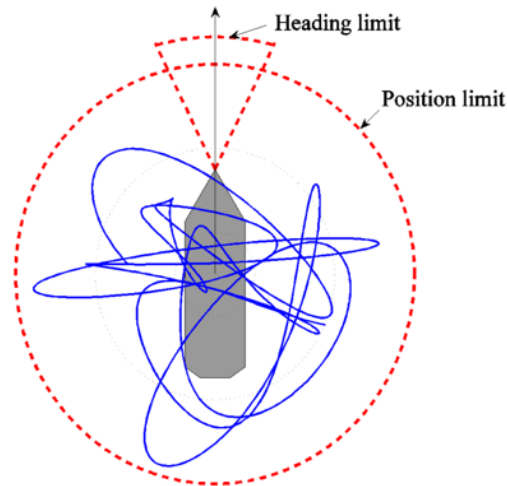
Figure 56 - Position and heading limits [40].

6.3.1 Simulations SK0

This is the first case of simulation and all the environmental conditions are zero. Due to this the system didn't move or rotated. Table 15 has these simulation conditions and Figure 57 shows the positioning and heading behavior.

Table 15 - Simulation SK0 conditions.

Heading	Beaufort number	DP capability number	Beaufort description	H_s (m)	T_p (s)	V_w (m/s)
0-360	0	0	Calm	0.00	0.00	0.00
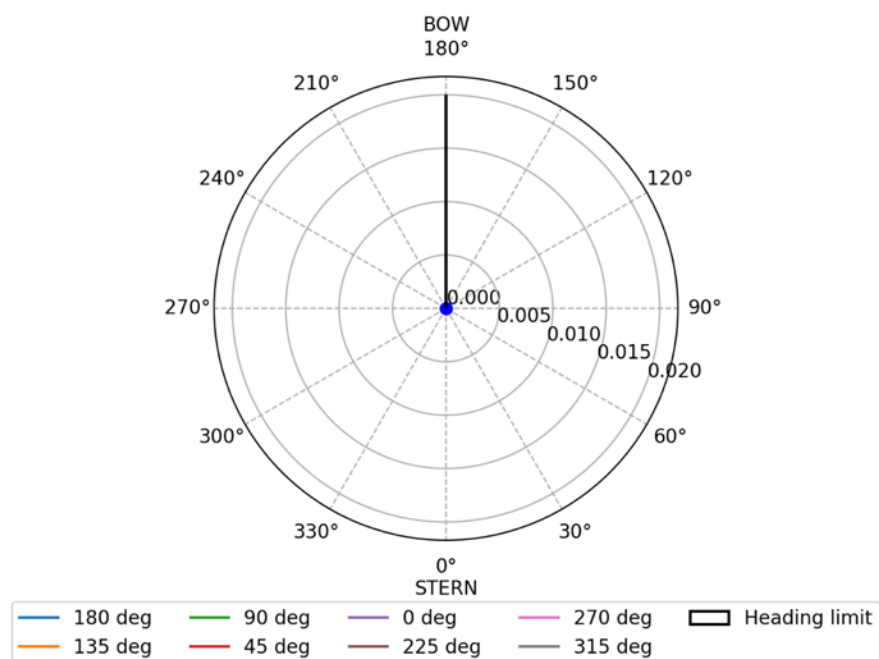
Figure 57 - Position and Heading limit output from simulation SK0.

Angular unit is degrees and the radial is meters.

6.3.2 Simulations SK1

In this second case, the autonomous system was under waves and wind and its behavior can be observed in Figure 58, which shows the positioning according to the environment incidence angle. Figure 58 also shows the heading limit for this case. Table 16 has these simulation conditions and behavior.

Table 16 - Simulation SK1 conditions.

Heading	Beaufort number	DP capability number	Beaufort description	H_s (m)	T_p (s)	V_w (m/s)
0-360	1	1	Light air	0.10	3.50	1.50
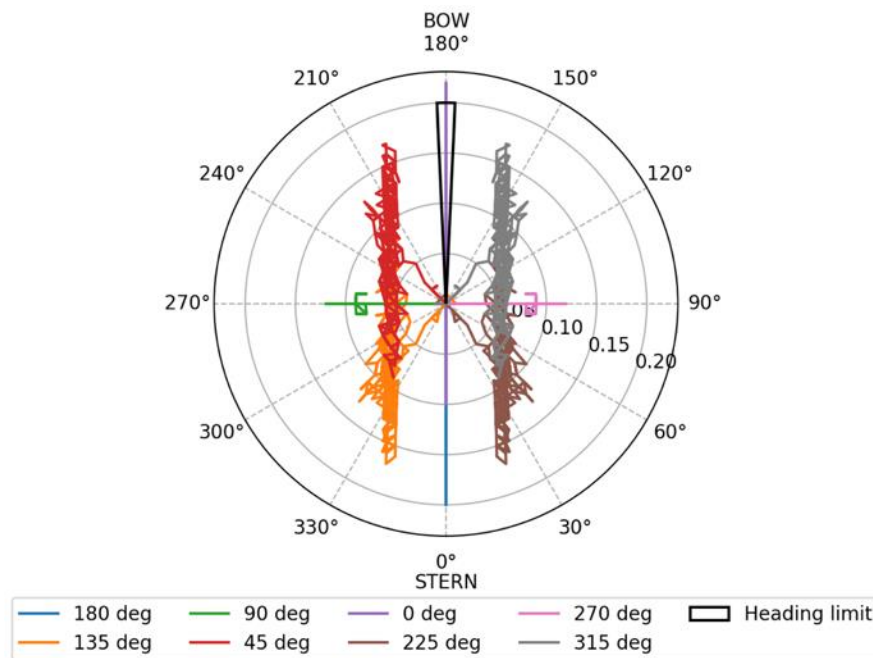
Figure 58 - Position and Heading limit output from simulation SK1.

Angular unit is degrees and the radial is meters.

It's important to notice that, for instance, when the waves and wind were being applied with an incidence angle of 45 degrees, the autonomous system moved (red line in Figure 58) first diagonally and then stayed oscillating around that position. Similar behavior can be observed in other incidence angles and cases.

6.3.3 Simulations SK2

Here the behavior is similar to the previous case, but with greater amplitude due to the more intense conditions. Table 17 has these simulation conditions and Figure 59 shows the positioning and heading behavior.

Table 17 - Simulation SK2 conditions.

Heading	Beaufort number	DP capability number	Beaufort description	H_s (m)	T_p (s)	V_w (m/s)
0-360	2	2	Litght breeze	0.40	4.50	3.40
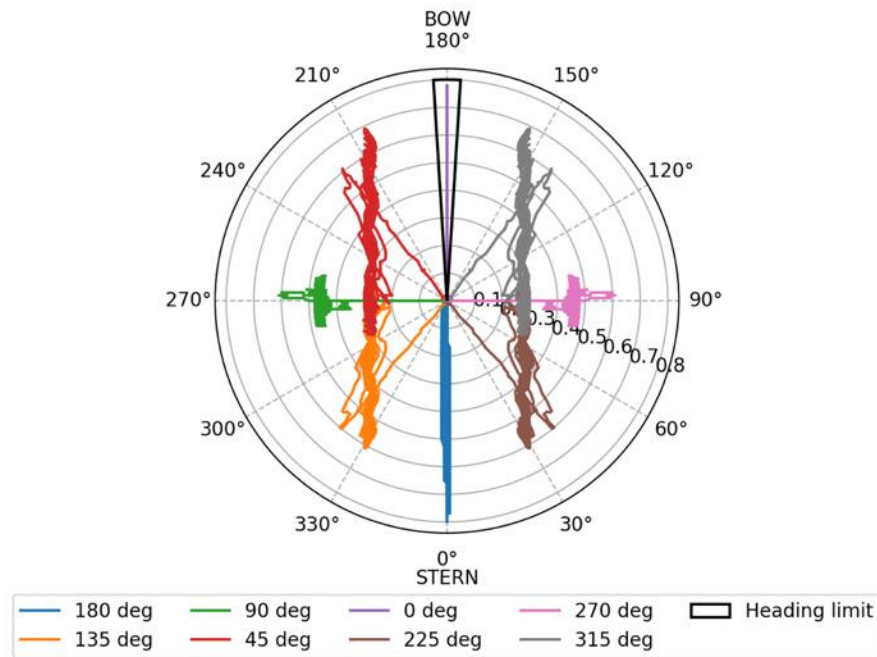
Figure 59 - Position and Heading limit output from simulation SK2.

Angular unit is degrees and the radial is meters.

6.3.3 Simulations SK3

This last case was the most intense that was simulated and we can observe that vessel's movement was around 1.6 meters in its worst case. In addition, the heading limit was lower than in the previous less intense cases. Table 18 has these simulation conditions and Figure 60 shows the positioning and heading behavior.

Table 18 - Simulation SK3 conditions.

Heading	Beaufort number	DP capability number	Beaufort description	H_s (m)	T_p (s)	V_w (m/s)
0-360	3	3	Gentle breeze	0.80	5.50	5.40
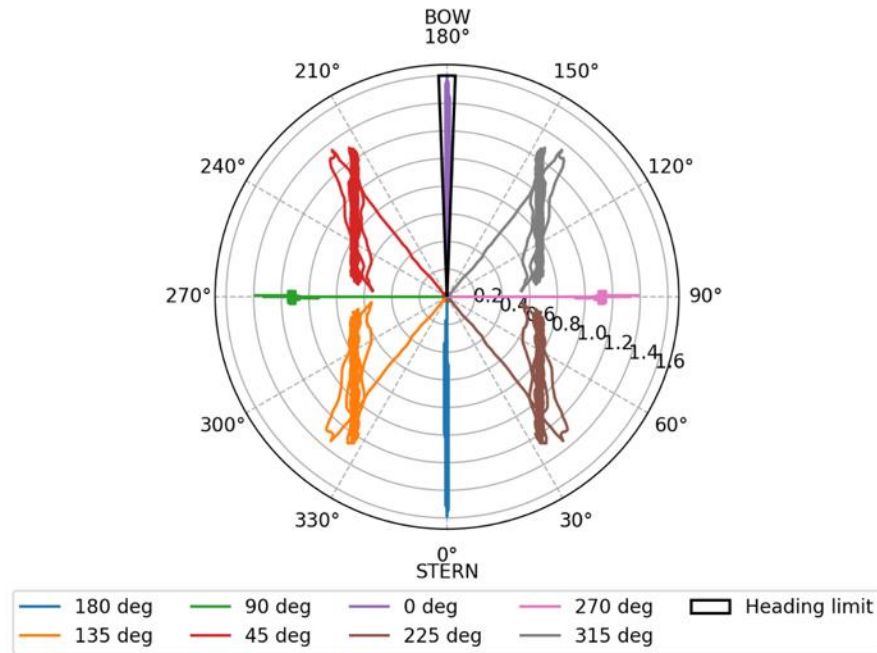
Figure 60 - Position and Heading limit output from simulation SK3.

Angular unit is degrees and the radial is meters.

6.3.1 Envelope

In order to better visualize the system behavior in different conditions, the envelope plot was built. This plot indicates the maximum translation and heading for each DP capability number condition. Table 19 summarizes all DP capability numbers conditions and Figure 61 shows the envelope plot.

Table 19 - DP capability numbers conditions.

Simulation	Heading	Beaufort number	DP capability number	Beaufort description	H_s (m)	T_p (s)	V_w (m/s)
SK0	0-360	0	0	Calm	0.00	0.00	0.00
SK1	0-360	1	1	Light air	0.10	3.50	1.50
SK2	0-360	2	2	Litght breeze	0.40	4.50	3.40
SK3	0-360	3	3	Gentle breeze	0.80	5.50	5.40
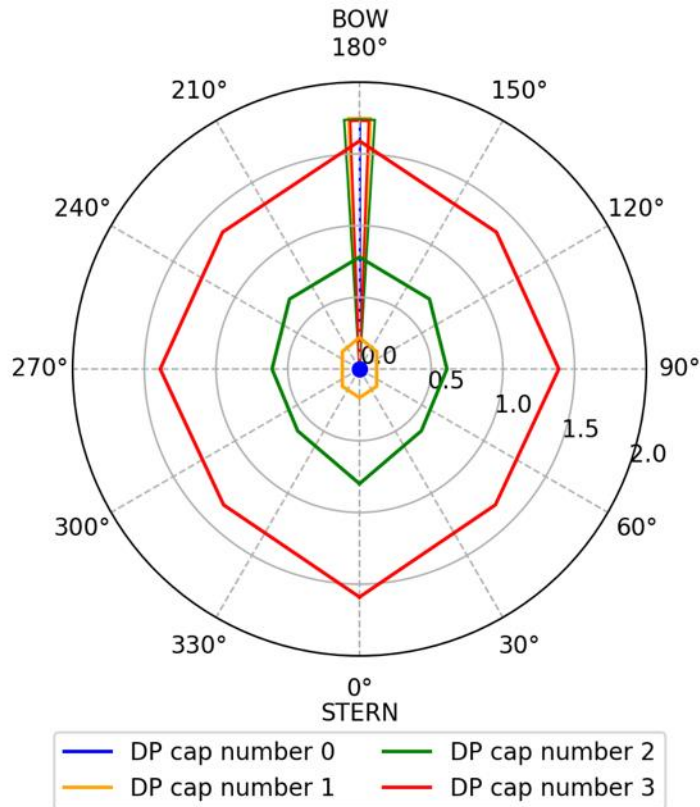
Figure 61 – Envelope plot of the DP capability numbers conditions for the autonomous system.

Angular unit is degrees and the radial is meters.

7 CONCLUSION

At this work, an initial project of an interchangeable autonomous propulsion system for small surface vessels was developed, verified and simulated. The system was designed so, all the items selected are available in Brazil and all software used are free, which means that a feasible and low-cost solution was proposed. The estimated cost of all components is around US$2,500.00.

The vessel's operational profile was tested for two cases: checking a ship's loaded draft marks and verifying the integrity of anchoring lines. Both cases simulated real conditions based on the location's data and known physical models. Also, usual noise values were added to the sensors, resulting in even more realistic conditions and a new motor speed controller logic was introduced. All these characteristics were successfully implemented and all the results showed a good agreement with the expectations and the strategy adopted.

Thinking about the essential necessity that this kind of platform has to keep its positioning, a station-keeping algorithm was implemented and simulated in different environmental conditions. These simulations were capable to generate great results that allow us to evaluate the performance of the autonomous platform against various circumstances, confirming its capacity for station-keeping.

Suggestions for future work, include:

- The integration between the station-keeping capability with the path-following algorithm, in order to have better results in more intense conditions during the path-following tasks;

- Implementation of a water current model to be used during the path-following and station-keeping simulations;

- Introduction of new sensors to measure wind and current speed to implement an algorithm to correct the drift during the tasks;

- Building the system and test experimentally in order to calibrate some coefficients (e.g. the wind coefficients) and have accurate results.

REFERENCES

[1] National Research Council. **Autonomous Vehicles in Support of Naval Operations**. Washington, DC: The National Academies Press, 2005.

[2] Weber, Marc. Computer History Museum. **Where to? A History of Autonomous Vehicles**. May 08, 2014. Disponível em:<https://computerhistory.org/blog/where-to-a-history-of-autonomous-vehicles/>. Acesso em: 19 fev. 2020.

[3] v2Gov. **da Vinci's Self-Propelled Cart: A Legacy of Autonomy**. Oct 10, 2017. Disponível em:<https://v2gov.com/da-vincis-self-propelled-cart/>. Acesso em: 20 fev. 2020.

[4] Science Encyclopedia. Science & Philosophy. **The Workings Of A Steam Engine**. Disponível em:< https://science.jrank.org/pages/6478/Steam-Engine-History.html >. Acesso em: 20 fev. 2020.

[5] Rigby, Rebecca. 19th Century Torpedoes. An annotated bibliography. **Whitehead, Robert (1823 - 1905)**. Disponível em:<http://www.torp.esrc.unimelb.edu.au/biogs/E000002b.htm>. Acesso em: 21 fev. 2020.

[6] Smithsonian Institution. **Wiley Post's Autopilot "Mechanical Mike"**. 2013. Disponível em:<https://airandspace.si.edu/multimedia-gallery/5074hjpg>. Acesso em: 21 fev. 2020.

[7] Kubota, Taylor. Stanford News. **Stanford's robotics legacy**. January 16, 2019. Disponível em:<https://news.stanford.edu/2019/01/16/stanfords-robotics-legacy/>. Acesso em: 21 fev. 2020.

[8] Delcker, Janosch. Politico. **The man who invented the self-driving car (in 1986)**. July, 2018. Disponível em:<https://www.politico.eu/article/delf-driving-car-born-1986-ernst-dickmanns-mercedes/>. Acesso em: 22 fev. 2020.

[9] BROWN, N. **More than just a remote possibility: USVs enter the fray**. Janes Navy International 109/1, pp.14-19, 2004.

[10] Bertram, V. **Unmanned Surface Vehicles: A Survey**. Singapore Maritime and Port Journal, 2006

[11] Evans, J. H. **Basic Design Concepts**. A.S.N.E Journal, Nov. 1959.

[12] Zoss, B.M. et al. **Distributed system of autonomous buoys for scalable deployment and monitoring of large waterbodies**. Auton Robot 42, 1669–1689, 2018.

[13] MURDIJANTO, Murdijanto; UTAMA, I Ketut; JAMALUDDIN, Andi. **An Investigation Into the Resistance/Powering and Seakeeping Characteristics of River Catamaran and Trimarana**. Makara Journal of Technology, [S.l.], v. 15, n. 1, p. 25-30, sep. 2011.

[14] Luhulima, R.B., Setyawan, D., & Utama, I.K. **Selecting Monohull , Catamaran and Trimaran as Suitable Passenger Vessels Based on Stability and Seakeeping Criteria**. The 14th International Ship Stability Workshop (ISSW), Kuala Lumpur, Malaysia, 2014.

[15] Magalhães, P.H.V. **Desenvolvimento de um submersível remotamente operado de baixo custo e caracterização dos sistemas de propulsão e vetorização de empuxo por hélice**. Tese de Doutorado, Universidade Federal de Minas Gerais, 2007.

[16] Sørdalen, O.J. **Optimal thrust allocation for marine vessels**. Control Engineering Practice, Volume 5, Issue 9, p. 1223-1231, 1997.

[17] Tannuri, E.A. **Desenvolvimento de metodologia de projeto de sistema de posicionamento dinâmico aplicado a operações em alto-mar**. Tese de Doutorado, Universidade de São Paulo, 2002.

[18] Zoss, B. M. **Design and analysis of mobile sensing systems: An environmental data collection swarm**. Master's thesis, Massachusetts Institute of Technology, 2016.

[19] Pereira, D.M., Antonio, A. **Navigation and guidance of an autonomous surface vehicle**. Master's thesis, University of Southern California, 2007.

[20] Fossen, T.I. **Guidance and control of ocean vehicles**. England: John Wiley & Sons Ltd, 1994.

[21] Fossen, T.I. **Handbook of Marine Craft Hydrodynamics and Motion Control**. United Kingdom: John Wiley & Sons Ltd, 2011.

[22] Ruane, P. (2014). **Heavenly mathematics: The forgotten art of spherical trigonometry**. United Kingdom: Princeton University Press, 2013.

[23] Mousazadeh, Hossein. **Experimental evaluation of a hydrography surface vehicle in four-navigation modes**. Journal of Ocean Engineering and Science, 2017.

[24] Sarda , E., Dhanak, M. **Unmanned recovery of an AUV from a surface platform**. pp. 1-6, MTS/IEEE San Diego, CA, 2013.

[25] Wilson, T., Williams, S.B. **Adaptive Path Planning for Depth Constrained Bathymetric Mapping with an Autonomous Surface Vessel**. J. Field Robotics, 35, 345-358, 2016.

[26] Bingham, B. **USV Plugins, Theory of Operation**. February 8, 2018.

[27] J. Tessendorf, C. C, and J. Tessendorf. **Simulating ocean water**. 1999.

[28] E. I. Sarda, H. Qu, I. R. Bertaska, and K. D. von Ellenrieder. **Station-keeping control of an unmanned surface vehicle exposed to current and wind disturbances**. Ocean Engineering, vol. 127, pp. 305 – 324, 2016.

[29] Inoue, S., Hirano, M., and Kijima, K. **Hydrodynamic Derivatives on Ship Manoeuvring**. International Shipbuilding Progress, vol. 28, pp. 112-125, 1981.

[30] Pandey, J., & Hasegawa, K. (2015). **Study on manoeuverability and control of an autonomous Wave Adaptive Modular Vessel (WAM-V) for ocean observation**. 2015 International Association of Institutes of Navigation World Congress (IAIN), 1-7.

[31] Triantafyllou, M.S., and Hover, F.S. **Maneuvering and Control of Marine Vehicles, Course notes for MIT course 2.154**. Maneuvering and Control of Marine Vehicles, Department of Mechanical Engineering, Massachusetts Institute of Technology, Cambridge, Massachusetts, 2001.

[32] Blevins, R.D. **Formulas for Natural Frequency and Mode Shape**. Robert E. kreiger Publishing Co. Malabar, FL, 1984.

[33] Tonon, D., Aronna, M.S., & Kalise, D. **Optimal control : novel directions and applications**. Springer, 2017.

[34] Svatoň, Martin. **Low-cost implementation of Differential GPS using Arduino**. 2016.

[35] Česenek, David. **Inertial measurement unit modeling**. 2019.

[36] Marquez, A.L. **Estudo de Agitação, Correntes Induzidas por Ondas e Balanço Sedimentar da Região do Porto de Tubarão e Praia de Camburí, Vitória/ES**. 2009.

[37] Bouças, I.A. **Estudo de Tensões em Costado de Fpso para a Avaliação da Vida à Fadiga**. 2016.

[38] Ferreira, L.H.S. **Comportamento Dinâmico de Estruturas Offshore**. 2015.

[39] Nascimento, M.X. **Análise das Condições Meteo-Oceanográficas na Região da Bacia de Santos**. 2013.

[40] Standard DNVGL-ST-0111. **Assessment of station keeping capability of dynamic positioning vessels**. Edition July 2016.